DNA demethylating agents suppress preclinical models of synovial sarcoma

Nobuhiko Hasegawa[1,2,3,4,#] , Nezha S. Benabdallah[5,6,7,8#], Kyllie Smith-Fry[1,2,3], Li Li[1,2,3], Sarah McCollum[1,2,3], Jinxiu Li[1,2,3], Caelen A. Jones[1,2,3], Lena Wagner[5,6,7], Vineet Dalal[5,6,7], Viola Golde[5,6,7], Anastasija Pejkovska[5,6,7], Lara Carroll[1,2,3], Malay Haldar[9], Seth M. Pollack[10], Scott W. Lowe[11,12], Torsten O. Nielsen[13], Ana Banito[5,6,7]*, Kevin B. Jones[1,2,3]*

[1] Department of Orthopaedics, University of Utah, Salt Lake City, UT, USA

[2] Department of Oncological Sciences, University of Utah, Salt Lake City, UT, USA

[3] Huntsman Cancer Institute, University of Utah, Salt Lake City, UT, USA

[4] Department of Orthopaedics, Juntendo University, Faculty of Medicine, Tokyo, Japan

[5] Hopp Children's Cancer Center, Heidelberg (KiTZ) Heidelberg, Germany

[6] German Cancer Research Center (DKFZ), Heidelberg, Germany

[7] National Center for Tumor Diseases (NCT), NCT Heidelberg, Germany

[8] Edinburgh Cancer Research, CRUK Scotland Centre, Institute of Genetics and Cancer, University of Edinburgh, Edinburgh, UK

[9] Department of Pathology and Laboratory Medicine, Perelman School of Medicine at the University of Pennsylvania, Philadelphia, PA, USA.

[10] Department of Medicine, Feinberg School of Medicine at Northwestern University, Chicago, IL, USA.

[11] Cancer Biology and Genetics Program, Memorial Sloan-Kettering Cancer Institute, New York, NY, USA.

[12] Howard Hughes Medical Institute, Chevy Chase, MD, USA.

[13] Department of Pathology and Laboratory Medicine, Vancouver Coastal Health Research Institute and Faculty of Medicine, University of British Columbia, Vancouver, BC, Canada.

[#]Hasegawa N and Benabdallah NS contributed equally as co-first authors.

*Correspondence should be addressed to:

Ana Banito, PhD

German Cancer Research Center (DKFZ)

Im Neuenheimer Feld 581

69120 Heidelberg, Germany

+49 6221 42 1581

a.banito@kitz-heidelberg.de

or

Kevin B. Jones, MD

2000 Circle of Hope Drive, Room 3726

Salt Lake City, Utah 84112, USA.

+1 801 585-0300

kevin.jones@hci.utah.edu

Running title: DNA demethylating agents are effective in synovial sarcoma.

Keywords: sarcoma, methylation, epigenetics

Abstract

Synovial sarcoma is an aggressive soft tissue cancer driven by the chimeric SS18::SSX fusion oncoprotein, which disrupts chromatin remodeling by combining two antagonistic transcriptional regulators. SS18 participates in BAF complexes that open chromatin, while the SSX genes are cancer-testis antigens that interface with chromatin decorated with monoubiquitinated histone H2A placed by Polycomb repressive complexes (PRCs) activity. Because KDM2B brings PRC to unmethylated CpG islands, it is plausible that methylation directly determines the distribution of SS18::SSX to target loci. Given that synovial sarcoma is also characterized by a peculiarly low DNA hypomethylation profile, we hypothesized that further disturbance of DNA methylation would have a negative impact on synovial sarcoma growth. DNMT1 disruption by CRISPR/Cas9 targeting or pharmacologic inhibition with cytidine analogs 5-aza-2′-deoxycytidine (decitabine) and 5-azacytidine led to decreased genome-wide methylation, redistribution of SS18::SSX, and altered gene expression profiles, most prominently including upregulation of tumor suppressor genes, immune-related genes, and mesenchymal differentiation-related genes. These drugs suppressed growth of synovial sarcoma cell lines and drove cytoreduction in mouse genetic models. DNMT1 inhibitors, already approved for treating myelodysplastic syndromes, warrant further clinical investigation for synovial sarcoma as repurposed, targeted treatments exploiting a vulnerability in the intrinsic biology of this cancer.

Introduction

Synovial sarcoma (SS) is a soft tissue sarcoma most frequently diagnosed in adolescents and young adults, with a third of all cases occurring in patients under the age of 20 (1). Current treatment strategies consist primarily of localized surgical resection often supported by (neo)adjuvant radiation therapy (2). Although systemic treatments, such as doxorubicin, ifosfamide, trabectedin, or pazopanib, are also frequently administered, they have limited impact on patient survival rates, which are poor after the development of progressive disease and metastasis (3). Despite these relatively poor treatment outcomes, the field of SS therapies has not drastically impacted the disease survivability in the past 30 years. Although the cellular therapy, afamitresgene autoleucel, was recently approved for SS, only a fraction of patients are eligible for this therapy, complete responses rate were very rare, and only a minority of patients experienced durable overall responses, all at the cost of high toxicity (4). This limited progress highlights the continuing need for innovative therapeutics in SS treatment, particularly any that can target the unique biology underlying this cancer of young populations.

SS belongs to the category of fusion gene-driven sarcomas, being defined by the chromosomal translocation t(X;18)(p11.2;q11.2), which leads to the formation of a fusion oncogene from which is expressed the fusion oncoprotein SS18::SSX (5, 6). This chimeric oncoprotein alone is sufficient to drive sarcomagenesis in the mouse, and is associated with a very low tumor mutational burden in humans and mice (7-12). SS18, the amino-terminal partner of this fusion protein, is a member of BAF (BRG1/BRM and Associated Factors) complexes, which are important chromatin remodelers involved in cell stemness and differentiation (13). The contributor of the carboxy terminus varies slightly, encoded by translocation to SSX1, SSX2, or, rarely, SSX4 (14, 15). The SSX proteins are considered

cancer-testis antigens, whose wildtype expression is often associated with spermatogenesis or malignancies (16-18). Among other potential mechanisms of action, the SSX carboxy termini interact with nucleosomes marked by histone post-translational modifications placed by Polycomb repressive complexes (PRCs), a family of important chromatin regulators. Upon expression of SS18::SSX, the fusion protein replaces wild-type SS18, becoming incorporated into the non-canonical GBAF (GLTSCR1-containing BAF) and canonical BAF complexes (19, 20). These events have major consequences, redirecting the BAF complex within the genome to alter transcription, ultimately resulting in tumorigenesis (19). While the driving mutation of SS is well characterized, the resulting fusion oncoprotein is not yet readily targetable with therapy. This renders any opportunity to target fusion-adjacent biology as an attractive potential therapeutic inroad.

We and others have recently shown that SS18::SSX is recruited to chromatin via its interaction with nucleosomes bearing monoubiquitinated lysine 119 of histone H2A (H2AK119ub), placed by PRC1.1 (21-23). Lysine demethylase 2 (KDM2B; also known as FBXL10 or JHDM1B) is the component of PRC1.1 responsible for loading the complex at precise genomic locations by recognizing and binding unmethylated CpG islands through its ZF-CxxC domain (24-26). KDM2B then drives the recruitment of other PRC1.1 components (BCOR, PCGF1, and RING1B/RNF2) to chromatin, placing H2AK119ub (26-28). SS has also been characterized as generally hypomethylated across its genome (11), and particularly at promoter sites (29).

Methylation inhibitors, including the cytidine analogs 5-aza-2′-deoxycytidine (DAC) and 5-azacytidine (5-AZA), have long been utilized in the treatment of hematologic malignancies, such as myelodysplastic syndrome (30). The mechanisms of antineoplastic

activity of demethylating agents are wide-ranging, including effects on apoptosis, differentiation, angiogenesis, senescence and other processes (31).

In many of their most efficacious uses, demethylating agents have induced the re-expression of genes, such as tumor-suppressor genes or neoantigens that were silenced by promoter methylation in the cancer cells (32). We speculated that the use of these drugs in SS may impact tumor development by further broadening and diluting the distribution of KDM2B and thus redistributing the SS18::SSX fusion oncoprotein to newly hypomethylated CpG islands, or by hypomethylating and activating the few genes that retain promoter hypermethylation as a means of silencing tumor suppressors or immune system recognized neoantigens.

Results

SS exhibits a dependency on DNMT1

Synovial sarcomas display a striking promoter DNA hypomethylation in which SS displays the lowest mean methylation level of any sarcoma. Importantly, this hypomethylation is specific to promoter regions and is not observed genome wide, in gene bodies or intergenic regions (29). Interestingly SS18::SSX has a known relationship with methylation profiles as its chromatin binding depends on the presence of KDM2B, the member of the PRCs that recognizes and binds unmethylated CpG islands (21). We therefore hypothesized that SS might be particularly sensitive to the removal of enzymes that regulate DNA methylation.

We first investigated whether the genes that regulate DNA methylation (*DNMT1, DNMT3A, DNMT3B, TET1, TET2, TET3)* are mis-expressed, mutated or amplified in SS. We performed *in silico* analysis using cBioPortal and DepMap public databases and compared mRNA expression levels and putative copy-number alterations among the same TCGA dataset of human soft tissue sarcomas: dedifferentiated liposarcoma (DDL, 50 cases), leiomyosarcoma (LMS, 53 cases), myxofibrosarcoma (MFS, 17 cases), SS (10 cases), and undifferentiated pleomorphic sarcoma (UPS, 44 cases). In SS, the mRNA expression levels of *DNMT1* and *DNMT3B* were similar to or lower than those in other sarcomas, whereas *DNMT3A* exhibited higher expression levels (Figure 1A). Expression levels of *TET* family genes that drive DNA demethylation were also higher in SS (Figure 1B) compared to other sarcoma subtypes. This corroborates recent findings showing elevated expression of *TET1* in human and murine SS when compared to normal cell counterparts (29). We did not observe prevalent copy number alterations or mutations in *DNMT* or *TET* genes in SS.

As higher levels of *TET1* expression are not associated with a dependency in synovial sarcoma (29), we sought to probe whether other enzymes are vulnerabilities. Using DepMap's RNA interference (RNAi) data across SS cell lines and the genes that orchestrate precise DNA methylation patterns, we observed that *DNMT1* is the only enzyme that displayed partial dependency with a gene effect (Chronos) value approaching −1 which is comparable to the median of all pan-essential genes (Figure 1C). We further confirmed that ChIP-seq data from our mouse genetic model identified the characteristic pattern of histone marks and fusion peaks around the *Tet3* locus that indicate it is directly targeted by the fusion oncoprotein (33), with similar—but less pronounced—marking of *Tet1* and *Dnmt3a* (Supplemental Figure 1). *Dnmt1*, *Dnmt3b*, and *Tet2* appear to be expressed with more of a housekeeping gene pattern of histone marks, less targeted by the fusion oncoprotein itself (Supplemental Figure 1).

CRISPR/Cas9 knockout of *DNMT1* using sgRNA (34) had a more negative impact on growth of an SS cell line (HS-SY-II) compared to an osteosarcoma cell line (KHOS) (Figure 1D). Although *sgDNMT1* strongly depleted SS cells over time, the slow pace of depletion is consistent with the requirement for passive loss of DNA methylation with each cell division in cancer cell lines that have relatively long doubling times.

Decitabine or *DNMT1* genetic disruption induces a mesenchymal-like phenotype

To evaluate the nature of the phenotypes caused by DNMT1 removal in synovial sarcoma, we targeted DNMT1 in SS human cell lines using sgRNA or decitabine, a cytidine analog that cannot be methylated and, after incorporation into DNA, progressively dilutes methylation markers in the chromatin of proliferating cells. Cells were evaluated at day 12

following *sgDNMT1* expression or decitabine treatment, allowing enough time for passive loss of DNA methylation.

We first confirmed knockout efficiency by assessing DNMT1 levels, showing an evident reduction upon transfection of sgRNA against *DNMT1* (Figure 2A). DNMT1 disruption or inhibition using 500 nM or 1 μM decitabine led to a global decrease in 5-methylcytosine (5mC) levels (Figure 2B).

Changes in methylation status can be monitored by evaluating the expression of certain methylation-sensitive genes, where promoter demethylation is followed by expected gene upregulation: *BCAS1, DAPK1, DNAH3, DNAH12,* and *ERC1* (35). 500 nM decitabine treatment was sufficient to recapitulate the *DNMT1* disruption phenotype in this gene set (Supplemental Figure 2A). Additionally, RNA sequencing results revealed similar expression profiles in cells treated with 500 nM decitabine or *DNMT1* disruption, indicating that the decitabine treatment had limited off-target effects (Supplemental Figure 2B). Collectively, these results suggest that 500 nM decitabine substantially decreases global methylation levels and mimics *DNMT1* disruption.

Gene expression was evaluated following treatment with decitabine, *sgDNMT1*, and *sgSSX*, as well as corresponding controls. The five major groups were divided into clusters A–E (Figure 2C). In cluster C, we selected those genes with a log2 fold-change of FPKM values greater than 0.5 compared to their controls and confirmed the overlap of *sgSSX*, *sgDNMT1*, and decitabine treatment. The other two groups are subsumed into the *sgSSX* group of upregulated expression genes (Supplemental Figure 2C). Comparison of *SS18::SSX* disruption to decitabine administration revealed that genes whose expression was downregulated by either had minimal overlap (Supplemental Figure 2D-E), whereas the genes upregulated in *SS18::SSX* disruption were also upregulated after decitabine treatment

(Figure 2D). Several genes were commonly upregulated in *sgDNMT1* and decitabine treatments in cluster C, with increased expression in *sgSSX* (Figure 2E). This cluster was enriched in extracellular matrix organization genes and other mesenchymal genes known to be expressed in fibroblasts. Accordingly, decitabine treatment triggered proliferative arrest and the acquisition of a fibroblast-like morphology in a manner that was substantially similar to the depletion or genetic disruption of *SS18::SSX1* (21). SS18::SSX function in mesenchymal lineage determination is likely partly mediated by DNA methylation of differentiation gene promoters. In HS-SY-II and SYO-1 cells, both decitabine administration and *sgSSX* showed similar impacts on cell morphology (Figure 2F, Supplemental Figure 2F). These observations indicate that reduced DNMT1-mediated genome methylation phenocopies some changes in SS morphology and cell growth associated with SS18::SSX depletion.

Synovial sarcoma cells exhibit sensitivity to DAC and 5-AZA

To determine whether DNMT1-mediated methylation landscape reprogramming can be used as a therapeutic strategy in SS, we performed a drug sensitivity test using decitabine or azacytidine in a panel of different SS cell lines, with two untransformed mesenchymal cell lines (KCO2 or MSCs) as controls (Figure 3A). All six SS cell lines (HS-SY-II, SYO-1, ASKA, MoJo, 1237/99, and YaFuSS) exhibit lower 50 percent inhibitory concentration (IC50) values for decitabine and azacytidine when compared to untransformed control cells. Additionally, IC50 levels were lower for decitabine when compared to azacytidine in SS lines, but, at higher concentrations, azacytidine exhibited a stronger cytotoxic effect than decitabine (Figure 3A). We compared HS-SY-II cells untreated, or treated with IC50-guided concentrations of decitabine- (500 nM), and azacytidine- (3 μM) for 6 days and measured

apoptosis and necrosis using a Caspase-3/7 green flow cytometry assay. Both treatments resulted in induction of apoptosis and necrosis, with azacytidine exhibiting a slightly higher necrosis percentage (Figure 3B). Finally, for an in vivo correlate of human cell line growth, we tested the SYO-1 cell line xenografted into the subcutaneous flanks of immunocompromised host mice (Figure 3C). Tumors harvested after treatment with decitabine were smaller than those treated with saline vehicle (Figure 3D, Supplemental Figure 3A). In histomorphology on hematoxylin and eosin stained sections of the xenograft tumors, the decitabine treatment group showed more spindled cell shapes and more collagenous matrix production, as further demonstrated on Masson's Trichrome (Supplemental Figure 3B and 3C). These results indicate that SS is sensitive to hypomethylation agents that in addition to growth arrest and induction of mesenchymal-related genes, they trigger at least some degree of growth inhibition by cell death.

Transcriptomic analysis of human SS cell lines treated with demethylases

To further explore the mechanisms by which decitabine and azacytidine inhibit tumor growth, we evaluated their effects on the transcriptome in HS-SY-II and SYO-1 cell lines. Principal component analysis (PCA) plot using transcripts per million (TPM) distinguished cell lines and treatments vs controls (Figure 4A). In HS-SY-II, decitabine treatment upregulated 1991 genes and downregulated 458 genes. Azacytidine treatment upregulated 1060 genes and downregulated 293 genes. A total of 923 upregulated genes were shared between the decitabine and azacytidine treatment groups, each relative to control, along with 152 shared downregulated genes (Figure 4B). In SYO-1, decitabine treatment upregulated 1498 genes and downregulated 1341 genes. Azacytidine treatment upregulated 593 genes and downregulated 467 genes in SYO-1. A total of 533 upregulated genes were shared between

the decitatine and azacytidine groups, along with 415 downregulated genes (Supplemental Figure 4A). From Gene Ontology (GO) analysis for each group, we constructed bubble plots by selecting the top 30 terms with the lowest *p*-values. Notably, in both cell lines treated with decitabine or azacytidine, GO terms related to nucleosome assembly were decreased, whereas those associated with extracellular matrix organization were increased (Figure 4C-D and (Supplemental Figure 4B).

Decitabine and azacytidine suppress tumor growth in synovial sarcoma mouse models

We next evaluated the effects of hypomethylating agents in SS tumors genetically-induced in mice with conditional expression of the *SS18::SSX2* fusion gene (Figure 5A) (9). Mice were treated with decitabine, azacytidine, or saline vehicle for 2 months and tumor growth was monitored by caliper measurements. Both agents suppressed tumor growth (azacytidine significantly), even achieving cytoreduction of some tumors (Figure 5B). Two-week treatment with decitabine or azacytidine also suppressed tumor growth for the subsequent 40 days after cessation of therapy; the decitabine group exhibited a rapid increase in tumor size, thereafter. In contrast, tumor growth suppression persisted for approximately 80 days in the azacytidine group following this brief treatment (Figure 5C).

Effects of decitabine and azacytidine on the transcriptome and methylome in mouse synovial sarcomas

RNAseq was also performed on tumors harvested after treatment in mice. A PCA map based on TPM showed separation based on histopathology sub-typing. Among the vehicle-treated samples, 1 and 3 were both biphasic/poorly differentiated tumors, whereas 2 was a monophasic tumor, and clustered distinctly. Among the decitabine-treated samples, 1 and 2 were both difficult to group into histological subtypes, as they clearly shrank during

treatment, leaving little evaluable tumor volume on representative histology sections. Decitabine-treated tumors 3 and 4 were biphasic and poorly differentiated, similar to the two vehicle-treated tumors. Of the azacytidine-treated samples, 1 and 2 were low-density monophasic spindle cell tumors based on the histology sections available. Conversely, 3 and 4 were biphasic / poorly differentiated tumors, similar to the two vehicle treated tumors, 1 and 3. Therefore, we selected for analysis the groups designated as VEH, AZA, DAC-A, and DAC-B (Figure 6A). In the RNAseq results, DAC-A tumors upregulated 221 genes and downregulated 383 genes relative to VEH tumors, highlighting many immune-related biological processes by GO analysis (Figure 6B). DAC-B treatment upregulated 1011 genes and downregulated 2060 genes, with extracellular matrix organization and skeletal system development featuring prominently in GO analysis (Figure 6C). AZA tumors upregulated 490 genes and downregulated 557 genes, featuring mostly skeletal development and extracellular matrix organization, but also some immune-related GO biological processes (Figure 6D). There were few shared genes between the DAC-A and AZA groups, 29 upregulated genes and 101 downregulated genes (Figure 6E). Focusing on the up-regulated groups in the Venn diagrams, we performed GO analysis (Supplemental Figure 5A and 5B). The GO analysis of the 29 genes in common included 4 genes involved in antigen presentation, 3 involved in response to viral infection, and another 3 involved in T cell-related immunity, indicating the induction of an immune response, overall (Supplemental Figure 5C). DAC-B and AZA groups shared 170 genes as commonly upregulated and 446 as commonly downregulated genes (Figure 6F). Similarly, we conducted an analysis focusing on groups with increased expression and found that the AZA-only upregulated genes were enriched for extracellular matrix organization (Supplemental Figure 5D). The AZA and DAC shared genes were enriched for synapse assembly (Supplemental Figure 5E). The DAC-only

upregulated genes were enriched for genes related to the skeletal system (Supplemental Figure 5F).

Decitabine and azacytidine alter SS18::SSX distribution

As SS18::SSX distributes according to the positioning of H2AK119ub, placed by the PRC1.1 complex, which is localized across the genome by KDM2B binding to unmethylated CpG islands, we investigated whether drug-induced changes in DNA methylation impact KDM2B genome occupancy as well as SS18::SSX chromatin binding (Figure 7A). Using ChIP-seq, we observed regions where decitabine treatment led to the acquisition of new or increased binding sites for SS18::SSX and KDM2B in HS-SY-II human SS cells that did not correspond to previous KDM2B sites (Figure 7B). Therefore, decitabine treatment led to a subtle diminution of SS18::SSX presence at a small subset of key regulatory elements, with subsequent rewiring and increased binding at new regions.

A similar phenomenon was clear from ChIP-seq for KDM2B in mouse SSs following treatment with vehicle or decitabine or azacytidine, with a diminution of the ChIP-seq enrichment at the promoters of known fusion target genes. The diminution of SS18::SSX itself was less consistent (Figure 7C). Only two examples of fusion target genes were identified that exhibited diminished KDM2B, diminished SS18::SSX, and diminished RNA-seq-determined expression (Figure 7D). Such patterns were not consistent across the bulk of fusion target genes, especially for their transcription, which was often increased, in spite of decreased fusion and KDM2B ChIP-seq enrichment. There are multiple potential

explanations for this inconsistency. First, it should be noted that even in tightly controlled cell lines, the diminution of fusion at typical target loci was subtle (Figure 7B). In whole tumor tissues, with intrinsic variability, this effect was even more difficult to detect with confidence. Second, the application of ChIP-seq to whole tumor samples from the mice tests as much the replacement of necrotic tumor cells with infiltrating fibroblasts and inflammatory cells as it tests the reprogramming of the neoplastic cells' chromatin. Most importantly, in the mouse tumors and human cell lines, while the redistribution phenomenon impacted KDM2B markedly, the target genes of the fusion did not significantly diminish in their transcription (see also Figure 2C, cluster B). There were other gained SS18::SSX binding sites without KDM2B binding that indicated the expression of novel genes from global hypomethylation that recruits canonical BAF complexes in which the fusion is more passenger than driver of recruitment to those sites. Overall, these results reject the hypothesized mechanism for reduced expression of canonical SS target genes by reduced recruitment of fusion and KDM2B to these loci. Instead, they indicate that due to the hypomethylated CpG islands in SS genomes, these cancer cells are more prone to aberrant gene activation by further global hypomethylation.

Further genome-wide hypomethylation upregulates gene expression

Histopathological analysis of the genetically-induced SSs in mice following treatment with decitabine or azacytidine revealed the typical treatment effects noted in human tumors following cytotoxic chemotherapy, including increased cytologic and nuclear atypia (characterized by enlarged nuclei, irregular chromatin and macronucleoli in treated tumor tissues), necrosis, and fibrous replacement of overtly neoplastic tissues (Figure 8A). Masson's trichrome staining was also performed, and sections from decitabine and azacytidine treated

mouse tumors stained with abundantly more collagenous matrix than those from vehicle treated tumors (Supplemental Figure 6A and 6B). Some such changes may be interpreted as conversion of neoplastic cells by derepressed differentiation, consistent with the increased expression of extracellular matrix genes in treated cell lines (Figure 4C-D). This interpretation of induced/permitted differentiation would better explain the appearance of even osteoid matrix production in extra-skeletal regions of genetically-initiated tumor treatments, due to the frequent observation of osteoid matrix in SS, but less commonly as a treatment effect in most other soft-tissue sarcoma types (36).

We performed integrated analyses of genome-wide methylation arrays, RNA-seq, and ChIP-seq to identify epigenetic changes associated with these therapeutic responses. Genes expressed at baseline that were not direct fusion targets and that were further hypomethylated by the two demethylase drugs were identified. We evaluated the DAC-B and AZA groups, which were characterized by extracellular matrix organization and skeletal system development in the RNA-seq GO analysis. The *NEAT1* and *RRAS* genes, which have been reported as tumor suppressor genes (37, 38) or positive regulators of angiogenesis (39) and skeletal muscle tissue development (40) showed substantial decreases in promoter methylation with either treatment (Figure 8B). RNA expression increased in both mouse tumors and human cell lines after drug administration or *DNMT1* disruption (Figure 8C). Focusing on genes related to the extracellular matrix (ECM), FLNB is a key factor involved in mesenchymal differentiation and ECM production. It is part of the cytoskeleton and also has documented gene regulatory functions, especially with regard to alternative splicing of RNA (41, 42). *FLNB* expression increased in conjunction with the decrease in methylation around the promoter (Supplemental Figure 6C and 6D). In ChIPseq, the SS18::SSX and KDM2B binding regions around the promoter are decreased, suggesting that the increased

transcription of this gene is not by a fusion-directed mechanism (Supplemental Figure 6E). In addition, in the drug administration groups, exon skipping was observed to have increased in two cell lines, upon treatment with either azacytidine or decitabine, and the expression of *FLNB* may be one reason for the effect on alternative splicing (Supplemental Figure 6F).

We also noted histology evidence of immune related activity in the treated tumors, ranging from hemosiderin-laden macrophages to infiltrating or clustered lymphocytes in or near the tumors (Figure 9A). We further evaluated the DAC-A and AZA groups, for promoter methylation and expression of immune-related genes identified in the RNAseq GO analysis. *ISG15, B2M*, and *MX2,* which are related to immunity (43-45), showed substantial decreases in promoter methylation and increases in RNA expression (Figure 9B-K).

Discussion

A primary goal in the study of any cancer cell is the identification of biology that is unique to the cancer and distinct from the host's normal cells. Targeting cancer cell specific biology with therapy will have a wide therapeutic window, where dosing of the agent can poison the cancer cell without harming the host. The biology of cancer cells provides a variety of categories of such targets, wherein it departs from normal cell biology in meaningful ways. In some instances, what is unique in the cancer cell is the presence or activity of some biology not shared by host cells. In other instances, it is the absence or inactivity of some biology in the cancer cells that host cells typically have present or active. In the adolescent and young adult malignancies driven by fusion oncoproteins, current therapeutic strategies have not targeted the unique fusion-associated biology as much as they have targeted pathways that are over- or under-represented in the cancer cells. Determining which biology is the better target, that which is over- or under-represented, is a philosophical challenge. Fortuitously, some of the epigenetic mechanisms that determine the reprogramming of gene expression in fusion oncoprotein-associated malignancies have proven to be vulnerabilities when pushed in either direction. This fine-tuning of such biological determinants has been termed the "Goldilocks principle" as related to expression levels of EWSR1::FLI1 in Ewing sarcoma, for example (46).

Here and in other related work, we have characterized profound genome hypomethylation as a unique biology that distinguishes SS from other sarcomas and most healthy cells of a host (29). Such hypomethylation might derive from overactive demethylating enzymes or underactive methylating enzymes. One could propose to target either of these therapeutically. In SS tumors, we found increased expression of demethylating enzymes and their targeting for upregulated transcription by the fusion oncoprotein (29).

However, single gene dependency testing identified only *DNMT1* among those two gene groups as a particular point of vulnerability, even if the observed state of SS suggested relatively low activity of this enzyme in the cancer cells.

We confirmed that application of purported DNMT1 inhibitors in SS cell lines strongly recapitulated the impact of *DNMT1* gene disruption in transcription and cell morphology in tissue culture. We also identified that such small molecule inhibitors are effective at suppressing growth of cell lines in culture or in a xenograft context. More strikingly, the drugs provided not only substantial growth suppression, but even cytoreduction in mouse genetically induced SSs. The persistent growth suppression that lasted for weeks after a brief period of drug application appears particularly promising for clinical translation of these agents to human patients with SS.

High expression of DNMT1 is associated with poor breast cancer survival and progression of disease (47-49). In many of the hematological malignancies for which DNMT1 inhibitors are used clinically, there is also elevated expression of the protein. This is not the case in SS, making its DNMT1 vulnerability somehow related instead to reduced baseline activity.

In our efforts to understand the mechanism of this sensitivity of SS to DNMT1 inhibitors, we tested a few potential mechanisms. Although the unique biology of fusion oncoprotein distribution across the chromatin of the genome depends on the hypomethylated state of developmental gene promoters, and further hypomethylation of other loci drove a redistribution effect on the fusion and reduction of its presence at typically targeted gene regulatory elements, this only rarely resulted in reduced expression of these target genes. Depletion of SS18::SSX only shared transcriptional downregulation with DNMT1 disruption or inhibition at a few genes. Instead, DNMT1 inhibition or disruption matched SS18::SSX

depletion in a subset of the genes which experienced upregulation from fusion depletion. The increased expression of non-fusion-targeted genes that were relatively suppressed transcriptionally at baseline in SS cells was the more prominent impact of the application of *DNMT1* silencing. These included genes that drove mesenchymal differentiation and extra-cellular matrix production, as well as tumor suppressor genes.

Further, while the epigenetic reprogramming characteristic of SS development already derepresses expression of several Cancer Testis Antigens (50, 51), the expression of these may be even more pronounced when demethylating agents are applied therapeutically. This likely explains some of the increased efficacy noted for these agents in our immune-competent mouse genetic models, over the xenografts of a human cell line.

Methods

Sex as a biological variable

For all mouse genetic model experiments, littermate controls were used, including randomly assigned male and female mice to each group. For the SYO-1 xenograft group, only female mice were used, as that cell line was derived from a tumor procured from a female patient. No sex-based differences were grossly observed in these experiments.

Cell lines

HS-SY-II, SYO-1, ASKA, YaFUSS, and 1273/99 cell lines were provided by M. Ladanyi, T. Nielsen, and Priya Chudasama (52-56). MoJo was generated in the laboratory (57). Human osteosarcoma KHOS-240S (RRID:CVCL_2544), Human Embryonic Kidney HEK293T (RRID:CVCL_0063), Immortalized human endometrial stromal cells KC02-44D hTERT (RRID:CVCL_E224) and were purchased from the American Type Culture Collection (ATCC). 1273/99 was cultured in RPMI 1640 (Gibco), other cell lines were cultured in Dulbecco's modified eagle medium (DMEM; Gibco) supplemented with 10% fetal bovine serum (FBS; Thermo Fisher) and 100 IU/mL penicillin/streptomycin (Gibco) and maintained in a humidified incubator at 37 °C with 5% CO_2ASC52telo, hTERT immortalized adipose derived Mesenchymal stem cells were purchased from ATCC (SCRC-4000) and were cultured in MesenPRO RS™ Medium (Gibco, 12746-012) supplemented with L-glutamine (Sigma-Aldrich, G7513-100ML). RAG MEF were procured from Scott Lowe's laboratory (MSKCC) and maintained in DMEM media supplemented with 10% Fetal Bovine Serum. Cells treated with 5-aza-2'-deoxycytidine (DAC) (Sigma) (stock 10 mM in DMSO) had the media changed every 48h for 6 days (growth assay) or 12 days (Dot Blot, RNA-seq, ChIP-seq).

Virus Production and transduction

Lentiviruses were produced by co-transfection of HEK293T cells. For a 6-well plate 1.10^6 cells were plated the day before transfection. 3µg constructs and helper vectors (2.5µg psPAX2 and 0.9µg VSV-G). Transfection of packaging cells was performed using Polyethylenimine (PEI) (Polysciences, 23966-2) by mixing with DNA in a 3:1 ratio. Viral supernatants were collected 48 after transfection, filtered through a 0.45 µm filter and supplemented with 4 µg /ml of polybrene (Sigma) before adding to target cells. Downstream experiments using DNMT1 sgRNAs knockout were performed 12 days after sgRNA induction.

Stable Cas9-expressing cell generation

HS-SY-II synovial sarcoma cell line was transduced with lentiCas9-Blast (58) (Addgene, #52962) and selected using 5 µg/ml of blasticidin to generate stable Cas9-expressing cell lines. Cells were consequently transduced with DNMT1 sgRNAs and selected with puromycin.

Plasmid Cloning

DNMT1 sgRNA for CRISPR knock-out were designed using Sanjana lab tool (http://guides.sanjanalab.org/) and cloned using their previously described protocol (34, 58). Briefly, sgRNAs were cloned by annealing two DNA oligos and ligating into a BsmB1-digested pLKO1-puro-U6-sgRNA-eGFP. Transformation was carried into Stbl3 bacteria.

Sequences are sgCTRL: CACCGTCCCATTCCTGGCCATTCT;

sgDNMT1 #1: CACCGCAGTCCTCTGTGAACACTG;

sgDNMT1 #2 CACCGCATCGAGATGTGGGACCCT

Western Blotting

Cells grown in 6-well plate were harvested and washed in PBS. Cell pellets were incubated with RIPA buffer (Cell Signalling) supplemented with protease inhibitors (Protease inhibitor tablets, Roche) for 30 min and cleared by centrifugation (15 min 14.000 rpms 4C). Protein lysates were quantified using the BCA protein assay (Pierce). Lysates were then denatured in 2X Laemmli (thermofisher) at 95C for 10 minutes and run in Mini-PROTEAN Precast Gels (BioRad) and transferred into membranes using Trans-Blot Turbo. Membranes then were blocked in 5% milk. The following antibodies were used for immunoblotting: β-Actin HRP clone AC-15 (A3854, Sigma), DNMT1 (D63A6) XP (#5032, Cell Signaling). Westerns were visualized using Amersham Imager 680.

Dot Blot

Genomic DNA from confluent 6-well plate was isolated using DNeasy Blood & Tissue Kits (Qiagen) according to manufacturer's protocol. DNA was resuspended in 50ul TE buffer. 1ug and 500ng DNA samples were added to up to 10 or 20ul of denaturation buffer (0.4 mM NaOH, 10 mM EDTA). DNA was denatured at 100°C for 10 min before being cooled on ice for 5 min. Samples were then applied to a positively charged nylon membrane under vacuum using a 96-well Dot Blot Hybridisation Manifold (Harvard Apparatus Limited) 2.5ul at the time and left to dry for 15 minutes. Membrane was then UV-cross-linked at 150mJ/cm2 and washed in 2X SSC. A second crosslink was applied, and membranes were left to dry for 6h at

room temperature. Membranes were then blocked in 10% Milk 1% BSA in PBT (PBS+0,1%Tween) Overnight at 4C. Hybond N+ membranes were probed with antibodies specific to OptimAb Anti-5-Methylcytosine (33D3) (BI-MECY-0100, Eurogentech, dilution factor 1:1000) for 1h at room temperature followed by Mouse IgG HRP Linked Whole Ab (NXA931, Sigma,1:10000) for 1h at RT. Membranes were then enhanced with chemiluminescence (ECL) and visualized using Amersham Imager 680. Methylene blue staining was carried out after this as loading control.

Cell Competition Assays

HS-SY-II and KHOS-240S Cas9 cells were transduced with an empty plasmid (Empty Vector) or a plasmid containing sgRNA targeting *DNMT1*. Infections were done with a virus dilution of 1:10 to obtain an infection efficiency of around 70-80%. Infected cells become GFP+ due to the backbone of the sgRNA. The cells were then cultured over a period of 25 days, and the percentage of GFP+ cells measured using a Fortessa FACS machine. Data was analysed using Flowjo software.

RNA extraction and Real Time quantitative Polymerase Chain Reaction (RT-qPCR)

RNA was prepared using RNeasy mini kit (Qiagen) according to manufacturer's protocol, including a DNaseI (Qiagen) treatment for 15mn at room temperature and cDNA was obtained using RevertAid First Strand cDNA Synthesis Kit (ThermoFisher).

Real-time PCR was carried on the Roche LightCycler 480 Real-Time PCR System using SYBR Green PCR Master Mix (Applied Biosystems). The relative expression of each sample was measured by the Lightcycler software and normalized to the mean for *Gapdh* from

replicates. Finally, the log2 of the ratio relative to dmso treated cells or safe guide induced cells was calculated when mentioned. Expression primers are the following: BCAS1(F), TTCTTCTGGTGTCCTGTGGA; BCAS1(R), TGGTAAGTCTCTGCTTCTGGT; DAPK1(F), GCAGGAAAACGTGGATGATT; DAPK1(R), CATTTCTTCACAACCGCAAA; DNAH3(F), GAACAACCTCCAGACGCG; DNAH3(R), TGGAAATGATATTCAGATGGCGA; DNAH12(F), CTCCCAACACATCCGACCAT; DNAH12(R), TTTTCCTGTGCCTGCTGG; ERC1(F), TGATTTTCTCTTGCTGCCGC; ERC1(R), CGCAATTCATCCTGGAGAGC.

RNA sequencing and data analysis of HS-SY-II cell line with CRISPR and decitabine

For high throughput RNA sequencing, total RNA from two independent experiments was extracted using a RNeasy mini kit (Qiagen). Cells transduced with the indicated sgRNAs or treated with DAC were collected 12 days post-infection. RNA-Seq library preparation and sequencing were performed at the High Throughput Sequencing Unit of the Genomics & Proteomics core facility of DKFZ using TruSeq Stranded Total RNA Library Prep kit (Illumina) and HiSeq 2000 v4 single-read 50bp sequencing system.

RNA seq reads were aligned the human genome assembly hg19 and FPKM count matrix was generated using featureCounts (59). Data analysis of replicate clustering (PCA analysis), heatmaps of the 5000 most variable genes and differential expression analysis were performed using iDEP (http://bioinformatics.sdstate.edu/idep93/) (60) . Sample-to-sample correlation heatmap was generated using DESeq2 (61).

RNA sequencing and data analysis of mouse model tumors and human cell lines

RNA was extracted from samples using TRIzol (Ambion, Inc., Life Technologies, Carlsbad, CA, USA; 15596018), followed by chloroform to 16.67% by volume. RNA was then purified from the suspended lysate and eluted in water using a kit (Zymo Research, Irvine, CA, USA; RNA Clean & Concentrator R1018).RNA-seq libraries prepared using a NEBNext Ultra II Directional RNA Library Prep with rRNA Depletion Kit (human,mouse,rat)(NEB) were sequenced on an IlluminaX Series 10B Reagent Kit_150x150 bp Sequencing (1250 M read-pairs/lane). The quality of raw paired-end sequence reads was assessed using FastQC. Low-quality (< 20) bases and adapter sequences were trimmed using Trimmomatic software (version 0.38) with the following parameters ILLUMINACLIP: path/to/adapter.fa:2:30:10 LEADING:20 TRAILING:20 SLIDINGWINDOW:4:15 MINLEN:36. The trimmed reads were aligned to the reference genome (mouse genome version mm10 and human genome version hg38) using the HISAT2 RNA-seq aligner (version 2.1.0). The raw read counts were normalized by relative log normalization (RLE) and differentially expressed analysis was conducted with DESeq2 (Version 1.24.0). The differentially expressed genes (DEGs) were detected with thresholds of |log2FC (fold change)| > 1 and adjusted *p*-value < 0.05 using the Benjamini–Hochberg (BH) method. GO enrichment analysis of DEGs was performed using GOATOOLS (version 1.1.6). Venn diagrams were plotted using the R package ggVennDiagram (version 1.2.0). Variance analysis was performed using the TPM values of

the RNA-seq data. Additionally, k-means clustering analysis was performed on the relevant genes identified using variance analysis. A heat map was plotted based on the k-means clustering analysis results.

Robust and flexible detection of differential alternative splicing from replicate (rMATS)

FASTQ files obtained from RNA sequencing of HS-SY-II and SYO-1 cells treated with azacytidine or decitabine were aligned to the reference genome, and splicing event quantification was performed using rMATS Turbo **(**version 4.1.2) (62). In this analysis, we used the JCEC (Junction Counts and Exon Coverage) mode to ensure comprehensive event detection, incorporating both exon inclusion and skipping events in the overall count estimation. The percentage spliced-in **(**PSI, Ψ) metric was used to measure the relative abundance of an exon in the spliced isoform. Statistically significant exon skipping (SE) events were identified based on an FDR (false discovery rate) threshold of <0.05, which was calculated using the Benjamini-Hochberg (BH) correction to control for multiple testing.

Immunofluorescence and Image Capture

HS-SY-II or SYO-I cells were seeded in 6-well plates at a density of 200,000 cells per well, and treated for 9 days with 500 nM Decitabine or corresponding amount of DMSO for the control. On day 9, the cells were re-suspended and seeded onto glass cover slips to allow for proper adherence. Treatment was performed for a total of 12 days. The cells were fixed with

4% PFA for 10 min at RT, permeabilized with 0.2% Triton X-100 in PBS 12 min at RT, and blocked with IF blocking solution (0.5% BSA and 0.2% fish skin gelatine in PBS) for 1h at RT. Incubation with the mouse β-ACTIN (ac-15, Sigma, 1:600) antibody was performed in blocking buffer for 1 hour at RT followed by incubation with anti-mouse-Alexa488 secondary antibody (A11001, Invitrogen, Thermofisher, 1:400) for 1h at RT. Alternatively, Phalloidin-Alexa647 (A22287, Invitrogen, Thermofisher) was diluted at 1:700 ratio in blocking solution and the samples were incubated with it for 1h at RT, followed by three washes with PBS. The slides were mounted in Vectashield antifade mounting medium with DAPI, sealed with clear nail polish, and imaged on an SP8 Leica confocal laser scanning microscope using a 40x oil immersion objective, 1024x1024 pixel image size, 100 Hz. Image analysis was performed using Fiji (ImageJ).

In vitro Drug Treatment

Cells were treated for 6 days and the drugs refreshed after 3 days. The viability assay was measure with Cell Titer Glow. Cells were seeded in duplicate at different numbers allowing growth for 6 days.

Calibrated Crosslinked Chromatin Immunoprecipitation (cChIP) in human cell lines

A modified ChIP protocol was used to analyze SS18-SSX1 binding in synovial sarcoma cells. HSSY-II cells with endogenously HA-tagged SS18-SSX and murine RAG-MEF cells overexpressing HA-SS18-SSX were cultured, with the latter used for spike-in controls. After 12 days of 500nM decitabine or DMSO treatment in triplicate, 10 million HSSY-II were

harvested and fixed using EGS (Thermo Fisher Scientific, #21565) and 1% formaldehyde (Thermo Fisher Scientific, #28908). Nuclei were isolated and sonicated using a Covaris ultrasonicator (M220). Each sample was sheared for 30 minutes at following conditions: Duty Factor = 10%, Peak Power = 75.0, Cycles/Burst = 200. Sheared chromatin was incubated with 5µg HA-Tag (C29F4) Rabbit mAb (#3724, Cell Signaling) per sample overnight at 4°C on a rotator, followed by immunoprecipitation using magnetic beads. After washing, DNA was purified using the Qiagen PCR purification kit (#28104).

Library preparation of human cell lines cChIP

DNA fragments obtained after ChIP were quantified using Qubit dsDNA HS Assay Kit (Invitrogen). 5ng of DNA was used for library preparation using NEBNext Ultra II DNA Library Prep Kit for Illumina (NEB, E7645S), SPRIselect beads (Beckman Coulter, #B23317) and NEBNext Multiplex Oligos for Illumina (NEB, Set 1 #E7335S) following NEB's guidelines (NEB, E7645S). All the libraries were done without size selection with an input of 5ng. ChIP libraries were sequenced as 50bp Paired-End reads on NovaSeq 6K SP.

cChIP-seq Analysis of human cell lines data

Raw reads were trimmed for quality and Illumina adapter sequences using trim-galore, then aligned to the human genome assembly T2T-CHM13 using Bowtie 2 (with "--very-sensitive" option). The spike-in data was analysed by aligning it to mouse genome mm10. The reads from the spike-in were used to normalise the reads. PCR duplicates were removed using Rmdup

tool. Down-sampling of reads for each sample was done based on the formula from Fursova et al. 2019:

Down-sampling factor: $\alpha \times {}^{1}/_{N(ChIP\ SpikeIn)} \times {}^{N(Input\ SpikeIn)}/_{N(Input\ HSSY)}$

Where α is a coefficient applied for all the files normalized together so the value of the largest down-sampling factor equals 1. N(ChIP SpikeIn) is the total number of reads aligned to the dm6 in the IP sample; N(Input SpikeIn) is the total number of reads aligned to mm10 in the corresponding Input; N(Input HSSY) is the total number of reads aligned to the T2T genome in the corresponding Input sample. The down-sampled replicates were then combined using the pileup function from MACS2 (q-value 0.05) and bigWig files were generated with ucsc-wigtobigwig tool. To visualize ChIP-Seq tracks, normalized bigWig files were generated with ucsc-wigtobigwig tool. Peaks were generated with the MACS2 callpeak function (with "--no model", "--qvalue 0.01", "--broad" options). CpG islands were imported from UCSC genome browser.

cChIP Data Visualisation of human cell lines data

Genome tracks were visualized using UCSC genome browser (https://genome.ucsc.edu/). For heatmaps and metaplot profiles read densities of the various IPs were centred around peak signals with a +/- 5 kb window from peak centre and binned with 50 bp using computeMatrix and plotProfile/plotHeatmap functions from deeptools.

Mouse genetic model of synovial sarcoma

The *Rosa26*^{hSS2} and *Myf5Cre* mouse strains were previously generated in our laboratory (9). Mouse tumor growth progression was measured using calipers and calculated using an ellipsoidal formula: volume = (length × width × width) × 0.5. Mice were monitored for signs of distress that indicated euthanasia via CO_2, followed by cervical dislocation. Tumors were surgically removed using sterilized scalpels and forceps, placed into 1.5-mL tubes, and immediately frozen in liquid N_2. The experiment included both male and female mice, with no observed differences between the two in the effects of drug treatments.

ChIP-sequencing of mouse model tumors

Snap-frozen tumor specimens were pulverized to near single-cell size with a hammer in the frozen state. For routine ChIP, pulverized tumors were thawed in phosphate-buffered saline (PBS) containing 1% formaldehyde and quenched with glycine (125 mM) after 10 min. Cells were pelleted and washed thrice with cold PBS. Nuclei were isolated by dousing in a solution of Tris-HCl (10 mM, pH 8.5), NaCl (10 mM), and NP-40 (0.5% volume) with protease inhibitor (PI, Sigma). They were then washed in a solution of Tris-HCl (10 mM, pH 8.5), NaCl (200 mM), EDTA (1 mM), and 1% SDS with PI. Nuclei were lysed at 4 °C in a solution of Tris-HCl (50 mM, pH 8.0), EDTA (10 mM), and 1% SDS with PI and immediately diluted 1:10 with a solution of 16.7 mM Tris-HCl pH 8.1, 16.7 mM NaCl, 1.2 mM EDTA, 1.1% Triton X-100, and 0.01% SDS with PI. Samples were sonicated with an EpiShear probe sonicator (Active Motif) at 40% amplitude for 8 cycles of 30 s each. Precipitated nuclear components that were not solubilized by sonication were centrifuged and removed. Dynabeads-Rabbit (30 μL; Thermofisher) were washed thrice in PBS with bovine serum albumin (BSA, 0.5 mg/mL), added to the sonicated chromatin, and incubated for 1 h at 4 °C for preclearance. The supernatant was transferred to a new tube. One subsample was set

aside as input. Sonicated chromatin was incubated with 5 µg of a primary antibody:anti-SS18::SSX (72364S, Cell Signaling) and KDM2B (17-10264, Sigma) overnight with rotation at 4 °C. The next day, 100 µL of the washed Dynabead slurry was incubated with the IPed chromatin for 4.5 h. The beads were then collected on a magnetic stand and washed sequentially with 6× ChIP RIPA buffer (10 mM Tris-HCI pH 7.5, 140 mM NaCl, 1 mM EDTA, 0.5 mM EGTA, 1% NP-40 or Triton X-100, 0. 1% SDS, and 0.1% NaDOC), 2× ChIP LiCl wash buffer (10 mM Tris-HCI pH 8.0, 1 mM EDTA, 500 mM LiCl, 0.5% NP-40, 0.5% NaDOC), and 1× with TE (10 mM Tris-HCI pH 8.0, 1 mM EDTA). Samples were eluted from the beads with buffer containing Tris-HCl (10 mM, pH 8.0), NaCl (150 mM), EDTA (5 mM), and SDS (1%). Cross-linking was reversed by adding and incubating with 40 µg of Proteinase K at 37 °C for 60 min and 65 °C for 3 h. DNA was purified using a DNA Clean & Concentrator Kit (Zymo). DNA was synthesized into sequencing libraries using the ChIP-Seq with NEBNext Ultra II DNA Library Prep Kit and then sequenced using NovaSeq X Series 10B Reagent Kit_150x150 bp Sequencing (1250 M read-pairs/lane).

ChIP-sequencing analysis of mouse model tumors

Reads were aligned to mm10 mouse genome version using Novoalign (Version 3.00) for paired-end reads. Peaks were called from each of the aligned bam files against input reads using MACS2 (63), (version 2.2.9) with the parameters: callpeak -B --SPMR --qvalue = 1e-3 --mfold 15 100. ChIP input was used as the background for MACS2. MACS was used to produce normalized bedgraphs, which were subsequently converted to bigWig files. Peaks were filtered to remove peaks that are in blacklist, including ENCODE blacklisted regions (64). Duplicate reads were removed using samtools rmdup for all downstream analyses (65).

Merged bigWig enrichment files for each condition with multiple replicas were generated in an average manner followed by normalization of read depth.

Heatmaps and profile plots that illustrate the scores corresponding to genomic regions were produced using the plotHeatmap function in deepTools (version 3.5.6) (66). This followed the computation of scores for each genomic region, a process which was executed using the computeMatrix function.

DNA methylation array

DNA methylation array experiments were performed using the Infinium Mouse Methylation BeadChip (Illumina). Approximately 500 ng of genomic DNA was bisulfite converted with the Zymo Research EZ DNA Methylation Kit (Illumina) with a slight modification. Samples were processed in a thermal cycler under the following conditions: 95 °C for 30 s, 50 °C for 60 min for 16 cycles, and held at 4 °C. Data were using the Infinium Mouse Methylation BeadChip and Illumina Infinium HD MouseMethylation-12 v1.0 arrays. Utilizing SeSAMe software (version 1.20.0), the beta and M values for each sample were obtained after general preprocessing of the idat file. The limma software was used to detect DMPs based on the M value. The probes with hyper (logFC > 1and p-values < 0.05) or hypo (logFC < -1and p-values < 0.05) methylated on AZA disposure and those on decitabine were compared, and their common and specific probes were identified.

GEMM drug treatment

Once tumors had developed to a size greater than 400 mm^3, animals were randomized into three groups, which received intraperitoneally administered vehicle (saline), 5 mg/kg DAC, or 5 mg/kg 5-AZA on four consecutive days/week. Tumor volume was calculated using the

following formula: 0.5 × (large diameter) × (small diameter)^2. The mice were sacrificed whenever a tumor's volume reached greater than 2000 mm^3.

Xenografts experiments

To generate xenografts, SYO-1 cells (15 × 10^6 per mouse flank) were harvested and injected in growth-factor-reduced Matrigel/PBS (50% final concentration). Each mouse flank was injected subcutaneously. Female 5- to 7-week-old athymic Nude-*Foxn1*^{nu} (Envigo) mice were used. Following inoculation, mice were monitored for tumor growth, and caliper measurements started when tumors became visible. Tumor volumes were calculated using the following formula: tumor volume = (D × d2)/2, in which D and d refer to the long and short tumor diameter, respectively. When tumors reached approximately 100mm3 decitabine treatment was initiated using 3 mg/kg i.p., 3 times/wk over two weeks. SYO-1-derived xenografts, tumors were harvested at the final time point and weighted. All mouse experiments were approved by the Memorial Sloan Kettering Cancer Center (MSKCC) Animal Care and Use Committee.

Tumor processing for histology

Tumor samples were fixed in 4% formaldehyde, dehydrated in serial ethanol solutions to xylene, embedded in paraffin, sliced into 4 μm sections with a microtome, and mounted on slides. Slides were deparaffinized with xylene, rehydrated with serial ethanol, and stained with hematoxylin and eosin or Masson's trichrome for light microscopy viewing.

Treatments and assessment of necrosis and apotosis by flow cytometry

To quantify necrosis and apoptosis, the CellEvent® Caspase-3/7 Green Flow Cytometry Assay Kit (Thermo) was used. Cells were labeled with CellEvent caspase 3/7 green detection reagent for 25 min at 37 °C; SYTOX AADvanced™ dead cell stain solution was added, and the cells were incubated for 5 min. A total of 10,0000 stained cells per sample were acquired and analyzed with a flow cytometer using Kaluza software ver 2.3 (Beckman Coulter).

Statistics

All statistical methods used were two-tailed and included a baseline level of significance threshold at $p < 0.05$. Graphs were created and analyzed using Prism Ten software (GraphPad). All quantitative data are presented as mean ± standard deviation. Methods used included the Mann–Whitney U test, and paired or homoscedastic t-tests (two-tailed, the latter for presumed equal variance, but not pairing), as noted in the figure legends.

Study approval

Mouse genetic model of synovial sarcoma experiments were performed with the approval of the University of Utah Institutional Animal Care and Use Committee and per international law and humane principles. All associated murine protocols were described under protocol 1442, last re-approved in November 2024.

Data availability

All underlying data used to generate the figures in this study are available in the file entitled "Supporting Data Values," which is provided as part of the Supplementary Information. All genomic data have been uploaded to the Gene Expression Omnibus under the accession GSE291441, 291301, 291302, 291312, 291314, and 292622.

Author contributions

NH, NSB, KSF, SM, JL, CAJ, LW, VD, VG, and AP performed experiments. NH, NSB, and LL analyzed data. LC, MH, SMP, SWL, TON, AB, and KBJ supervised experiments and designed analyses. The paper was written primarily by NH, NSB, TON, AB, and KBJ and edited by all authors.

Acknowledgments

All were supported by National Cancer Institute (NIH) U54CA231652. T.O.N. is supported by Canadian Institutes for Health Research grant 025845.

N.S.B. was supported by a DKFZ Postdoctoral Fellowship.

N.H. is supported by JSPS KAKENHI Grant Number 23KK0310.

A.B. was supported by the European Research Council (ERC) under the European Union's Horizon 2020 research and innovation programme (805338).

We thank the antitumor assessment core facility (MSKCC) and the MSK cancer center support grant (P30 CA008748) for assistance with experiments using human synovial sarcoma xenografts.

Disclosure statement

The authors have declared that no conflict of interest exists.

References

1. Eilber FC, and Dry SM. Diagnosis and management of synovial sarcoma. *J Surg Oncol.* 2008;97(4):314-20.

2. Mangla A, and Gasalberti DP. *StatPearls*. Treasure Island (FL): StatPearls Publishing

3. Blay JY, von Mehren M, Jones RL, Martin-Broto J, Stacchiotti S, Bauer S, et al. Synovial sarcoma: characteristics, challenges, and evolving therapeutic strategies. *ESMO Open.* 2023;8(5):101618.

4. D'Angelo SP, Araujo DM, Abdul Razak AR, Agulnik M, Attia S, Blay JY, et al. Afamitresgene autoleucel for advanced synovial sarcoma and myxoid round cell liposarcoma (SPEARHEAD-1): an international, open-label, phase 2 trial. *Lancet.* 2024;403(10435):1460-71.

5. Turc-Carel C, Dal Cin P, Limon J, Rao U, Li FP, Corson JM, et al. Involvement of chromosome X in primary cytogenetic change in human neoplasia: nonrandom translocation in synovial sarcoma. *Proc Natl Acad Sci U S A.* 1987;84(7):1981-5.

6. Sandberg AA, and Bridge JA. Updates on the cytogenetics and molecular genetics of bone and soft tissue tumors. Synovial sarcoma. *Cancer genetics and cytogenetics.* 2002;133(1):1-23.

7. Barrott JJ, Kafchinski LA, Jin H, Potter JW, Kannan SD, Kennedy R, et al. Modeling synovial sarcoma metastasis in the mouse: PI3'-lipid signaling and inflammation. *J Exp Med.* 2016;213(13):2989-3005.

8. Chalmers ZR, Connelly CF, Fabrizio D, Gay L, Ali SM, Ennis R, et al. Analysis of 100,000 human cancer genomes reveals the landscape of tumor mutational burden. *Genome medicine.* 2017;9(1):34.

9. Haldar M, Hancock JD, Coffin CM, Lessnick SL, and Capecchi MR. A conditional mouse model of synovial sarcoma: insights into a myogenic origin. *Cancer Cell.* 2007;11(4):375-88.

10. Jones KB, Barrott JJ, Xie M, Haldar M, Jin H, Zhu JF, et al. The impact of chromosomal translocation locus and fusion oncogene coding sequence in synovial sarcomagenesis. *Oncogene.* 2016;35(38):5021-32.

11. Comprehensive and Integrated Genomic Characterization of Adult Soft Tissue Sarcomas. *Cell.* 2017;171(4):950-65.e28.

12. Nacev BA, Sanchez-Vega F, Smith SA, Antonescu CR, Rosenbaum E, Shi H, et al. Clinical sequencing of soft tissue and bone sarcomas delineates diverse genomic landscapes and potential therapeutic targets. *Nat Commun.* 2022;13(1):3405.

13. Hargreaves DC, and Crabtree GR. ATP-dependent chromatin remodeling: genetics,

genomics and mechanisms. *Cell Res.* 2011;21(3):396-420.

14. Clark J, Rocques PJ, Crew AJ, Gill S, Shipley J, Chan AM, et al. Identification of novel genes, SYT and SSX, involved in the t(X;18)(p11.2;q11.2) translocation found in human synovial sarcoma. *Nat Genet.* 1994;7(4):502-8.

15. Ladanyi M. Fusions of the SYT and SSX genes in synovial sarcoma. *Oncogene.* 2001;20(40):5755-62.

16. Gure AO, Türeci O, Sahin U, Tsang S, Scanlan MJ, Jäger E, et al. SSX: a multigene family with several members transcribed in normal testis and human cancer. *International journal of cancer.* 1997;72(6):965-71.

17. dos Santos NR, Torensma R, de Vries TJ, Schreurs MW, de Bruijn DR, Kater-Baats E, et al. Heterogeneous expression of the SSX cancer/testis antigens in human melanoma lesions and cell lines. *Cancer Res.* 2000;60(6):1654-62.

18. Smith HA, Cronk RJ, Lang JM, and McNeel DG. Expression and immunotherapeutic targeting of the SSX family of cancer-testis antigens in prostate cancer. *Cancer Res.* 2011;71(21):6785-95.

19. Li J, Mulvihill TS, Li L, Barrott JJ, Nelson ML, Wagner L, et al. A Role for SMARCB1 in Synovial Sarcomagenesis Reveals That SS18-SSX Induces Canonical BAF Destruction. *Cancer Discov.* 2021;11(10):2620-37.

20. Kadoch C, and Crabtree GR. Reversible disruption of mSWI/SNF (BAF) complexes by the SS18-SSX oncogenic fusion in synovial sarcoma. *Cell.* 2013;153(1):71-85.

21. Banito A, Li X, Laporte AN, Roe JS, Sanchez-Vega F, Huang CH, et al. The SS18-SSX Oncoprotein Hijacks KDM2B-PRC1.1 to Drive Synovial Sarcoma. *Cancer Cell.* 2018;33(3):527-41.e8.

22. McBride MJ, Mashtalir N, Winter EB, Dao HT, Filipovski M, D'Avino AR, et al. The nucleosome acidic patch and H2A ubiquitination underlie mSWI/SNF recruitment in synovial sarcoma. *Nat Struct Mol Biol.* 2020;27(9):836-45.

23. Tong Z, Ai H, Xu Z, He K, Chu GC, Shi Q, et al. Synovial sarcoma X breakpoint 1 protein uses a cryptic groove to selectively recognize H2AK119Ub nucleosomes. *Nat Struct Mol Biol.* 2024;31(2):300-10.

24. Farcas AM, Blackledge NP, Sudbery I, Long HK, McGouran JF, Rose NR, et al. KDM2B links the Polycomb Repressive Complex 1 (PRC1) to recognition of CpG islands. *Elife.* 2012;1:e00205.

25. He J, Shen L, Wan M, Taranova O, Wu H, and Zhang Y. Kdm2b maintains murine embryonic stem cell status by recruiting PRC1 complex to CpG islands of developmental genes. *Nat Cell Biol.* 2013;15(4):373-84.

26. Wu X, Johansen JV, and Helin K. Fbxl10/Kdm2b recruits polycomb repressive complex

1 to CpG islands and regulates H2A ubiquitylation. *Mol Cell.* 2013;49(6):1134-46.

27. Junco SE, Wang R, Gaipa JC, Taylor AB, Schirf V, Gearhart MD, et al. Structure of the polycomb group protein PCGF1 in complex with BCOR reveals basis for binding selectivity of PCGF homologs. *Structure.* 2013;21(4):665-71.

28. Wong SJ, Gearhart MD, Taylor AB, Nanyes DR, Ha DJ, Robinson AK, et al. KDM2B Recruitment of the Polycomb Group Complex, PRC1.1, Requires Cooperation between PCGF1 and BCORL1. *Structure.* 2016;24(10):1795-801.

29. Hofvander J, Qiu A, Lee K, Bilenky M, Carles A, Cao Q, et al. Synovial Sarcoma Chromatin Dynamics Reveal a Continuum in SS18:SSX Reprograming. *bioRxiv.* 2024.

30. Ma J, and Ge Z. Comparison Between Decitabine and Azacitidine for Patients With Acute Myeloid Leukemia and Higher-Risk Myelodysplastic Syndrome: A Systematic Review and Network Meta-Analysis. *Front Pharmacol.* 2021;12:701690.

31. Howell PM, Liu Z, and Khong HT. Demethylating Agents in the Treatment of Cancer. *Pharmaceuticals (Basel).* 2010;3(7):2022-44.

32. Jones PA, and Baylin SB. The fundamental role of epigenetic events in cancer. *Nat Rev Genet.* 2002;3(6):415-28.

33. Li J, Li L, Smith-Fry K, Wilmot ZF, Carroll L, Morrison L, et al. SS18::SSX redistributes BAF chromatin remodelers selectively to activate and repress transcription.

bioRxiv. 2024:2024.05.14.594253.

34. Shalem O, Sanjana NE, Hartenian E, Shi X, Scott DA, Mikkelson T, et al. Genome-scale CRISPR-Cas9 knockout screening in human cells. *Science.* 2014;343(6166):84-7.

35. Brocks D, Schmidt CR, Daskalakis M, Jang HS, Shah NM, Li D, et al. DNMT and HDAC inhibitors induce cryptic transcription start sites encoded in long terminal repeats. *Nat Genet.* 2017;49(7):1052-60.

36. Barrott JJ, Illum BE, Jin H, Hedberg ML, Wang Y, Grossmann A, et al. Paracrine osteoprotegerin and β-catenin stabilization support synovial sarcomagenesis in periosteal cells. *J Clin Invest.* 2018;128(1):207-18.

37. Xiao R, Shi L, Yang T, Zhang M, Wang H, and Mai S. Identification of RRAS gene related to nasopharyngeal carcinoma based on pathway and network-based analyses. *Transl Cancer Res.* 2019;8(2):664-75.

38. Ghafouri-Fard S, and Taheri M. Nuclear Enriched Abundant Transcript 1 (NEAT1): A long non-coding RNA with diverse functions in tumorigenesis. *Biomed Pharmacother.* 2019;111:51-9.

39. Komatsu M, and Ruoslahti E. R-Ras is a global regulator of vascular regeneration that suppresses intimal hyperplasia and tumor angiogenesis. *Nat Med.* 2005;11(12):1346-

50.

40. Wang S, Zuo H, Jin J, Lv W, Xu Z, Fan Y, et al. Long noncoding RNA Neat1 modulates myogenesis by recruiting Ezh2. *Cell Death Dis.* 2019;10(7):505.

41. Ma HR, Cao L, Wang F, Cheng C, Jiang R, Zhou H, et al. Filamin B extensively regulates transcription and alternative splicing, and is associated with apoptosis in HeLa cells. *Oncol Rep.* 2020;43(5):1536-46.

42. Wang X, Jia Q, Yu L, Huang J, Wang X, Zhou L, et al. Filamin B knockdown impairs differentiation and function in mouse pre-osteoblasts via aberrant transcription and alternative splicing. *Heliyon.* 2024;10(20):e39334.

43. Perng YC, and Lenschow DJ. ISG15 in antiviral immunity and beyond. *Nat Rev Microbiol.* 2018;16(7):423-39.

44. Wang H, Liu B, and Wei J. Beta2-microglobulin(B2M) in cancer immunotherapies: Biological function, resistance and remedy. *Cancer Lett.* 2021;517:96-104.

45. Juraleviciute M, Nsengimana J, Newton-Bishop J, Hendriks GJ, and Slipicevic A. MX2 mediates establishment of interferon response profile, regulates XAF1, and can sensitize melanoma cells to targeted therapy. *Cancer Med.* 2021;10(8):2840-54.

46. Seong BKA, Dharia NV, Lin S, Donovan KA, Chong S, Robichaud A, et al. TRIM8 modulates the EWS/FLI oncoprotein to promote survival in Ewing sarcoma. *Cancer*

Cell. 2021;39(9):1262-78.e7.

47. Mirza S, Sharma G, Parshad R, Gupta SD, Pandya P, and Ralhan R. Expression of DNA methyltransferases in breast cancer patients and to analyze the effect of natural compounds on DNA methyltransferases and associated proteins. *J Breast Cancer.* 2013;16(1):23-31.

48. Jahangiri R, Jamialahmadi K, Gharib M, Emami Razavi A, and Mosaffa F. Expression and clinicopathological significance of DNA methyltransferase 1, 3A and 3B in tamoxifen-treated breast cancer patients. *Gene.* 2019;685:24-31.

49. Yu Z, Xiao Q, Zhao L, Ren J, Bai X, Sun M, et al. DNA methyltransferase 1/3a overexpression in sporadic breast cancer is associated with reduced expression of estrogen receptor-alpha/breast cancer susceptibility gene 1 and poor prognosis. *Mol Carcinog.* 2015;54(9):707-19.

50. Iura K, Maekawa A, Kohashi K, Ishii T, Bekki H, Otsuka H, et al. Cancer-testis antigen expression in synovial sarcoma: NY-ESO-1, PRAME, MAGEA4, and MAGEA1. *Hum Pathol.* 2017;61:130-9.

51. Vanacker H, Connacher R, Meurgey A, Bollard J, Attignon V, Tirode F, et al. Brief Communication on MAGE-A4 and Coexpression of Cancer Testis Antigens in Metastatic Synovial Sarcomas: Considerations for Development of

Immunotherapeutics. *J Immunother.* 2025;48(1):27-31.

52. Sonobe H, Manabe Y, Furihata M, Iwata J, Oka T, Ohtsuki Y, et al. Establishment and characterization of a new human synovial sarcoma cell line, HS-SY-II. *Lab Invest.* 1992;67(4):498-505.

53. Kawai A, Naito N, Yoshida A, Morimoto Y, Ouchida M, Shimizu K, et al. Establishment and characterization of a biphasic synovial sarcoma cell line, SYO-1. *Cancer Lett.* 2004;204(1):105-13.

54. Nojima T, Wang YS, Abe S, Matsuno T, Yamawaki S, and Nagashima K. Morphological and cytogenetic studies of a human synovial sarcoma xenotransplanted into nude mice. *Acta Pathol Jpn.* 1990;40(7):486-93.

55. Ishibe T, Nakayama T, Okamoto T, Aoyama T, Nishijo K, Shibata KR, et al. Disruption of fibroblast growth factor signal pathway inhibits the growth of synovial sarcomas: potential application of signal inhibitors to molecular target therapy. *Clinical cancer research : an official journal of the American Association for Cancer Research.* 2005;11(7):2702-12.

56. Xie Y, Skytting B, Nilsson G, Gasbarri A, Haslam K, Bartolazzi A, et al. SYT-SSX is critical for cyclin D1 expression in synovial sarcoma cells: a gain of function of the t(X;18)(p11.2;q11.2) translocation. *Cancer Res.* 2002;62(13):3861-7.

57. Jin H, Barrott JJ, Cable MG, Monument MJ, Lerman DM, Smith-Fry K, et al. The Impact of Microenvironment on the Synovial Sarcoma Transcriptome. *Cancer Microenviron.* 2017;10(1-3):1-7.

58. Sanjana NE, Shalem O, and Zhang F. Improved vectors and genome-wide libraries for CRISPR screening. *Nat Methods.* 2014;11(8):783-4.

59. Liao Y, Smyth GK, and Shi W. featureCounts: an efficient general purpose program for assigning sequence reads to genomic features. *Bioinformatics.* 2014;30(7):923-30.

60. Ge SX, Son EW, and Yao R. iDEP: an integrated web application for differential expression and pathway analysis of RNA-Seq data. *BMC Bioinformatics.* 2018;19(1):534.

61. Anders S, and Huber W. Differential expression analysis for sequence count data. *Genome Biol.* 2010;11(10):R106.

62. Shen S, Park JW, Lu ZX, Lin L, Henry MD, Wu YN, et al. rMATS: robust and flexible detection of differential alternative splicing from replicate RNA-Seq data. *Proc Natl Acad Sci U S A.* 2014;111(51):E5593-601.

63. Zhang Y, Liu T, Meyer CA, Eeckhoute J, Johnson DS, Bernstein BE, et al. Model-based analysis of ChIP-Seq (MACS). *Genome Biol.* 2008;9(9):R137.

64. An integrated encyclopedia of DNA elements in the human genome. *Nature.*

2012;489(7414):57-74.

65. Li H, Handsaker B, Wysoker A, Fennell T, Ruan J, Homer N, et al. The Sequence Alignment/Map format and SAMtools. *Bioinformatics.* 2009;25(16):2078-9.

66. Ramírez F, Ryan DP, Grüning B, Bhardwaj V, Kilpert F, Richter AS, et al. deepTools2: a next generation web server for deep-sequencing data analysis. *Nucleic Acids Res.* 2016;44(W1):W160-5.

Figure Legends

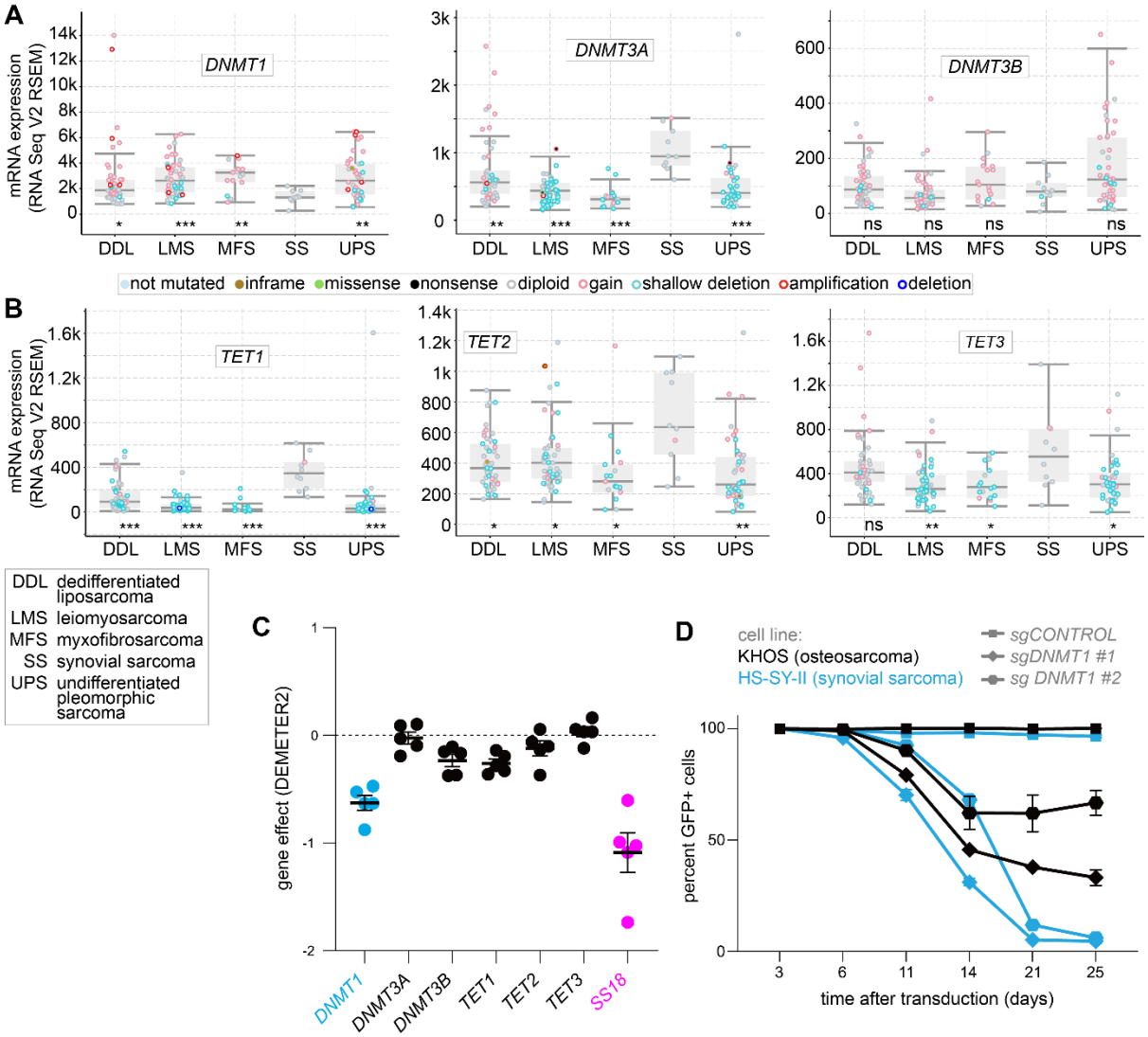

Figure 1. The synovial sarcoma genome is hypomethylated by increased TET and decreased DNMT1 expression. (**A**) *DNMT1*, *DNMT3A*, and *DNMT3B* mRNA expression and mutational profile from cBioPortal analysis. Expression levels for 20,532 genes in 264 soft tissue cases (RNA Seq V2 RSEM). GISTIC 2.0; -2 = deep deletion; -1 = shallow deletion; 0 = diploid; 1 = gain; 2 = amplification. *p* values were determined by Mann–Whitney U test. *p < 0.05, **p < 0.005, ***p < 0.0005 ; ns., not significant. (**B**) *TET1, TET2*, and *TET3* mRNA expression and mutational status. (**C**) Gene-specific dependence scores for each SS cell line in the Target Drive initiative accessed by DepMap. (**D**) Cell competition assay performed in the osteosarcoma cell line KHOS-240S-Cas9 (fusion negative control) or in the synovial sarcoma line HS-SY-II-Cas9 transduced with a safe sgRNA as control or with guides targeting DNMT1.

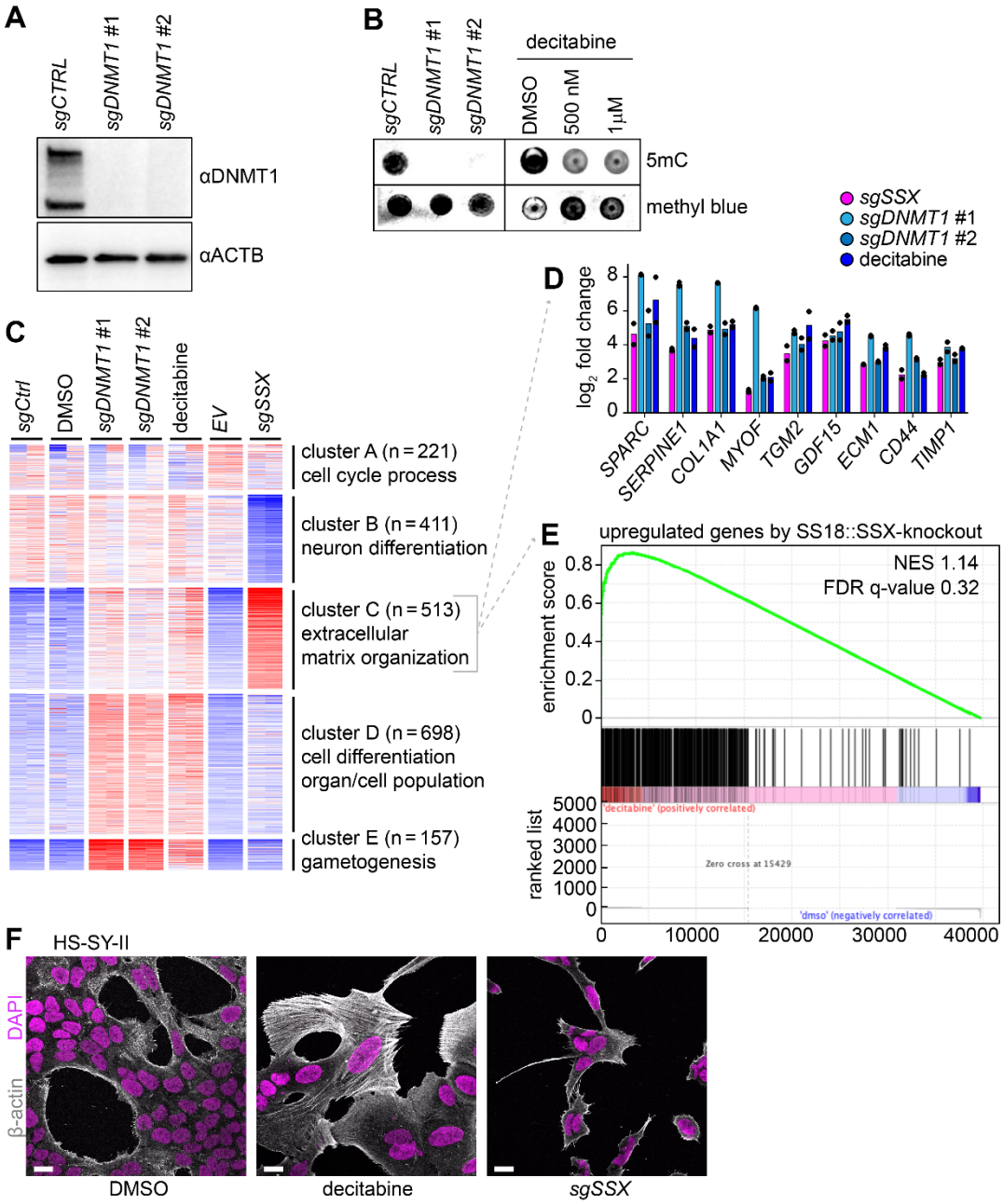

Figure 2. Decitabine treatment mimics *DNMT1* knockout and leads to mesenchymal-like phenotype. (**A**) Western Blot of whole cell extract from HS-SY-II-Cas9 expressing either a safe sgRNA (CTRL) or sgRNAs targeting DNMT1 for 12 days revealed with either anti-DNMT1 or anti-β-actin antibodies. (**B**) Global methylation levels measured by 5mC methylation dot blot using 1ug genomic DNA and methyl blue as loading control. (**C**) Heatmap of transcriptional analysis heatmap showing K-means clustering of the 2000 most variable genes with a cutoff z-score of 4 in HS-SY-II-Cas9 expressing sgRNAs safe (CTRL) or targeting DNMT1 or HS-SY-II treated with either DMSO or 500nM Decitabine for 12 days. n = 2. (**D**) Log2 fold change of FPKM values from genes present in cluster C, extracellular matrix organization. Data represent the mean of two biological replicates. (**E**) Gene set enrichment analysis (GSEA) comparing the expression of the 513 genes present in cluster C with the top 500 genes upregulated upon SS18-SSX knockout. (**F**)

Immunofluorescence of human synovial sarcoma HS-SY-II cells stained with DAPI (magenta) and beta-actin (grey). Scale bar represents 20μm throughout the panel.

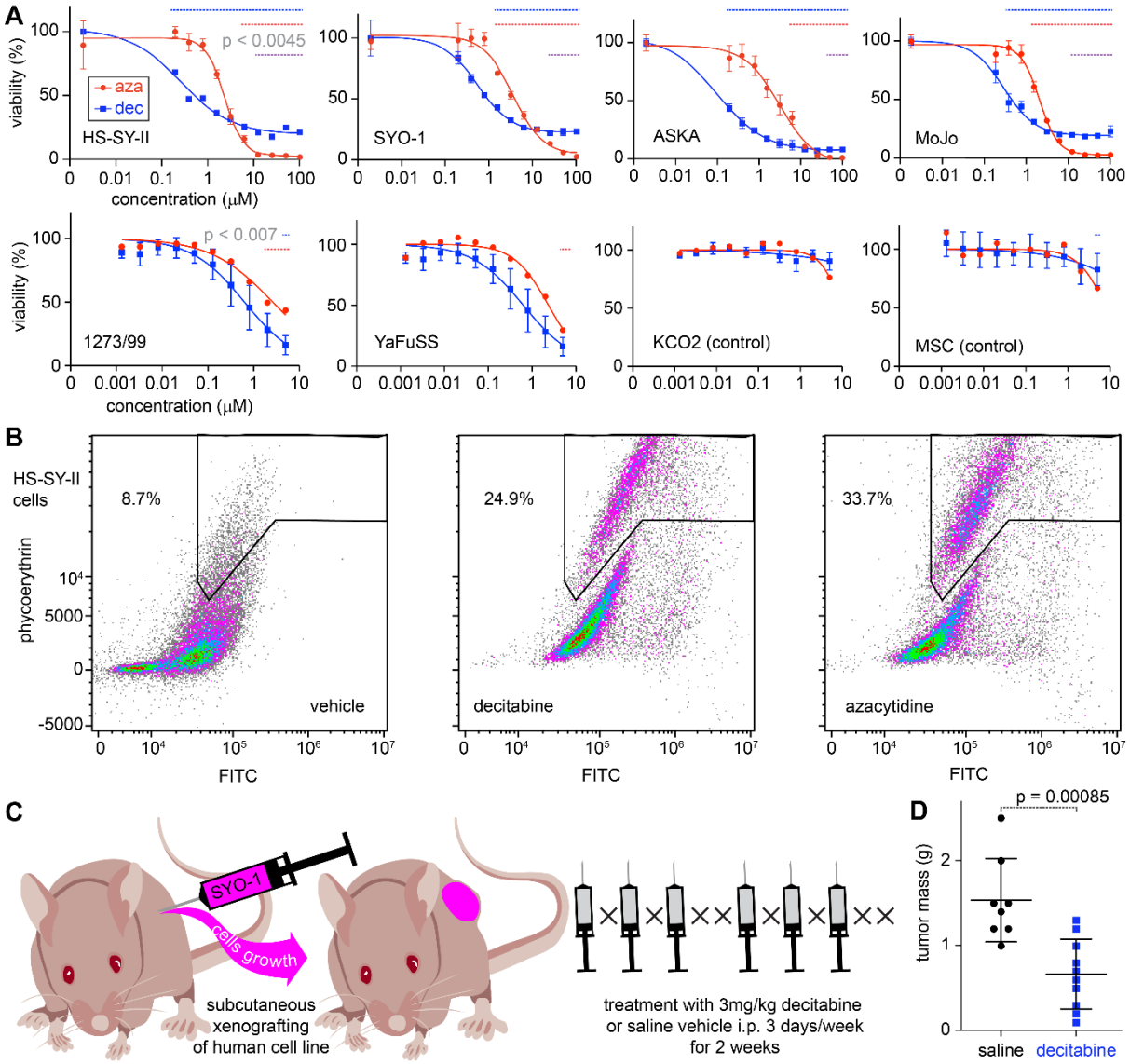

Figure 3. Synovial sarcoma is sensitive to decitabine and azacytidine. (**A**) Viability of six synovial sarcoma cell lines and two untransformed mesenchymal cell lines treated with decitabine or azacytidine. The blue dotted line indicates the points where the *p* value of the cell survival rate compared to the reference point in decitabine is significant. The red dotted line indicates the comparison to the reference for azacytidine. (1273/99, YaFuss, KCO2, and MSC are compared based on pooling of the initial two points.) The purple dotted line indicates the significantly different regions in each point of decitabine and azacytidine in HS-SY-II, SYO-1, ASKA, and MoJo. In MoJo, one outlier values of more than 5 times the DAC at 100uM were excluded. *p* values were determined by two-tailed paired t-tests. (*p* values of less than 0.0045 were considered significant in the upper row, less than 0.007 for the lower row, each Bonferroni corrected from 0.05). (**B**) Necrosis areas similarly framed for control (vehicle), decitabine-, and azacytidine-treated groups. (**C**) Diagram of a xenograft mouse model and details of drug administration. (**D**) Comparison of tumor mass after 2 weeks of treatment. *p* value was determined by two-tailed homoscedastic t-test. (n = 8 control, n = 10 decitabine treatments)

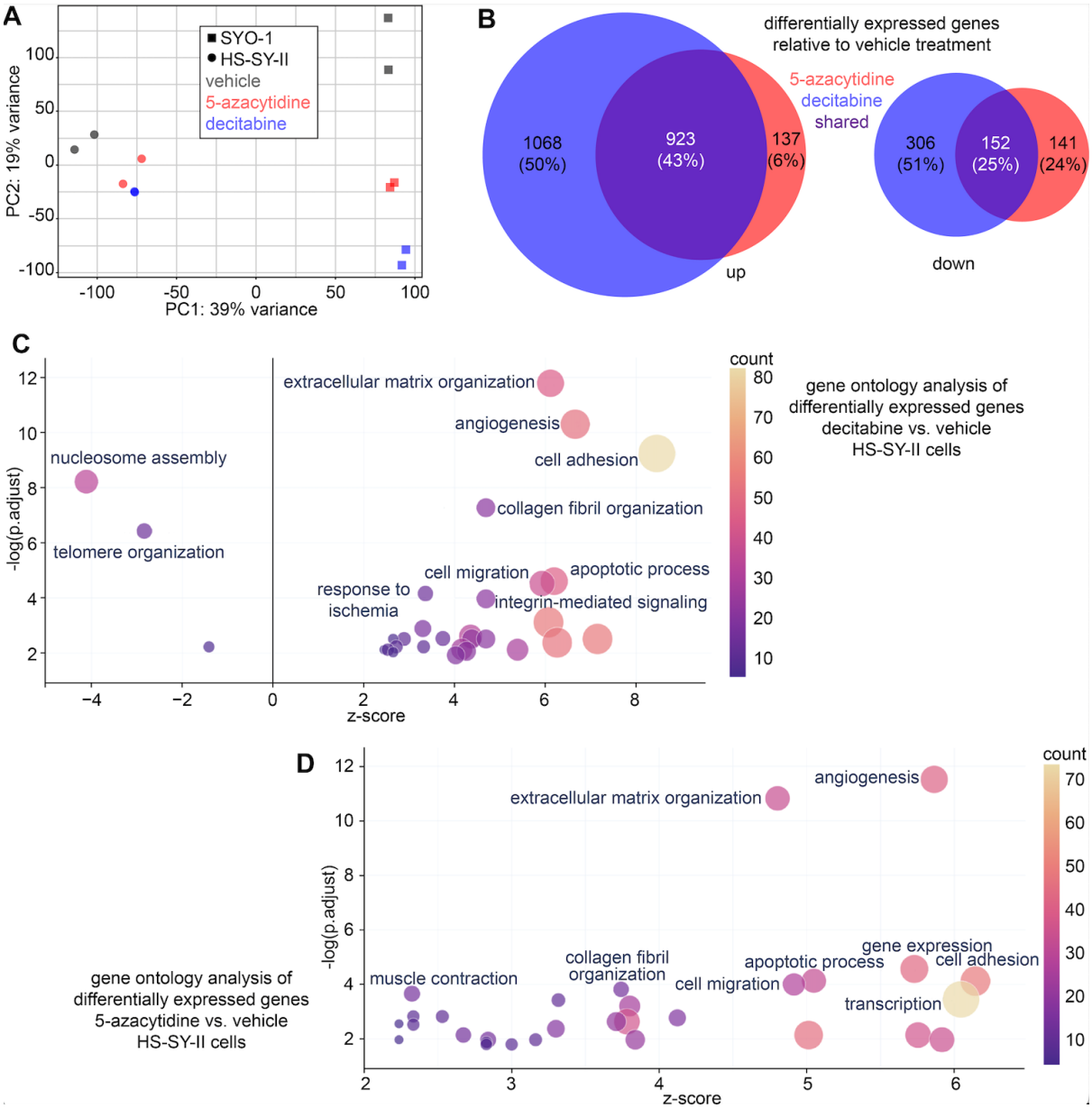

Figure 4. Transcriptomes change from decitabine or azacytidine applied to human synovial sarcoma cell lines. (**A**) TPM-based principal component analysis of whole transcriptomes. (**B**) Genes with expression variation log2 fold-change expression (<-1/>1) and adjusted $p < 0.05$; (left) group with increased expression, (right) group with decreased expression. (**C**) Bubble plots from GO analysis of up- and downregulated genes in HS-SY-II cells following decitabine treatment compared to vehicle. (**D**) GO analysis of upregulated genes and the biological processes in HS-SY-II cells following 5-azacytidine treatment.

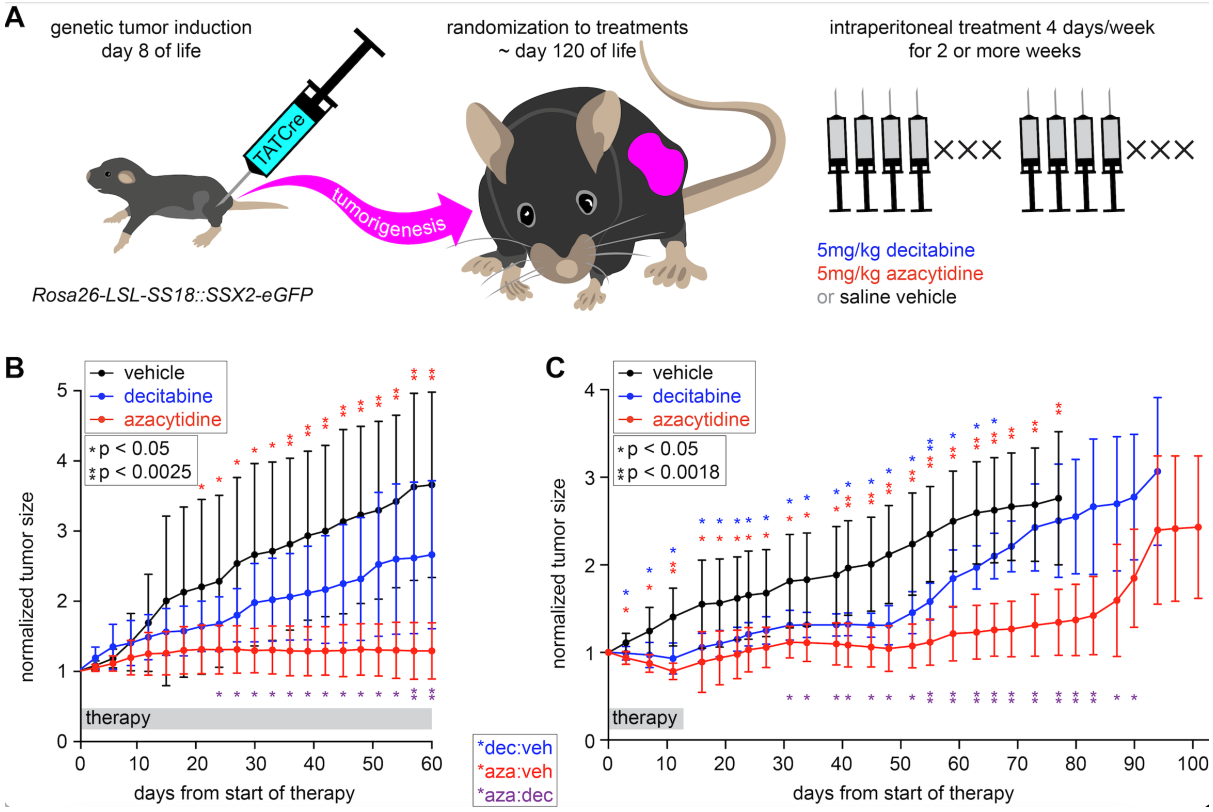

Figure 5. Decitabine and azacytidine treatments impact genetically induced synovial sarcomas in mice. (**A**) Diagram of a genetically induced mouse model and details of drug administration. (**B**) Tumor growth curves for each group. Normalized (fractional) tumor volumes are presented as mean ± SD. Two-tailed homoscedastic t-test *p* values less than 0.05 are indicated with a single asterisk, those less than the Bonferroni corrected *p*-value are indicated with a double asterisk (red for azacytidine compared to vehicle, purple for azacytidine compared to decitabine; n = 8 for vehicle and decitabine treatments, and 10 for azacytidine treatments). (**C**) Course of normalized mean tumor size from day 0 of treatment, administered for 14 days and then stopped. Two-tailed homoscedastic t-test *p* values less than 0.05 are indicated with a single asterisk, those less than the Bonferroni corrected *p*-value are indicated with a double asterisk (blue for decitabine compared to vehicle, red for azacytidine compared to vehicle, purple for azacytidine compared to decitabine; n = 9 for azacytidine and decitabine treatment groups, and 5 for the vehicle control group).

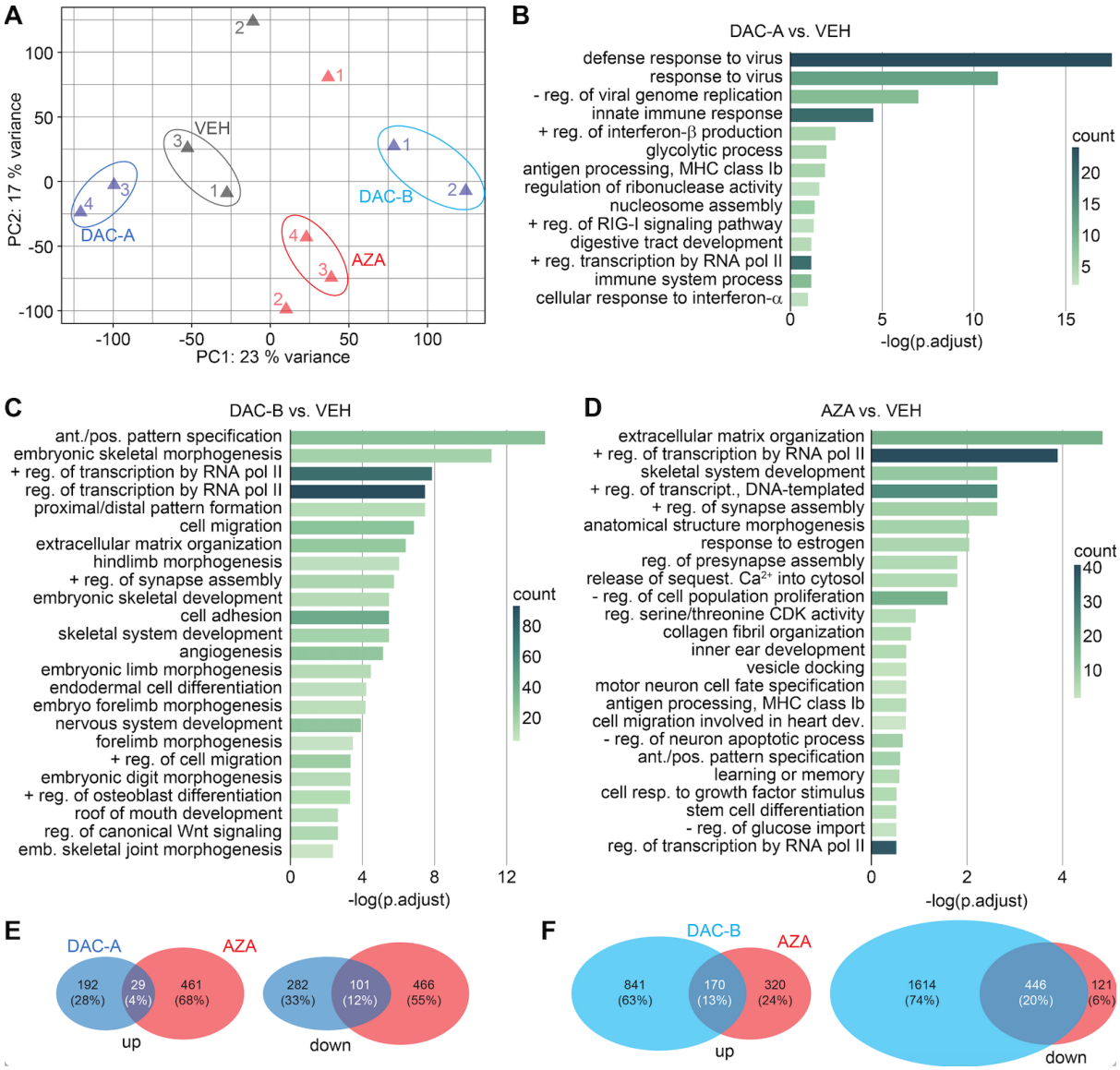

Figure 6. Transcriptional changes by pharmacological demethylation in genetically induced mouse synovial sarcomas. (A) TPM-based PCA**.** Decitabine samples were classified by histology into two groups, DAC-A and DAC-B. (**B**) GO terms for biological processes for genes with upregulated differential expression log2 fold-change (<-1/>1) and adjusted $p < 0.05$ in DAC-A compared to VEH group. (**C**) GO analysis of the biological processes in DAC-B over VEH upregulated genes. (**D**) GO analysis of the biological processes in gene upregulated in AZA group tumors compared to VEH. (**E**) Venn diagrams of shared upregulated and downregulated genes each relative to VEH of DAC-A and AZA groups. (**F**)Venn diagrams for shared genes between DAC-B and AZA, each compared to VEH.

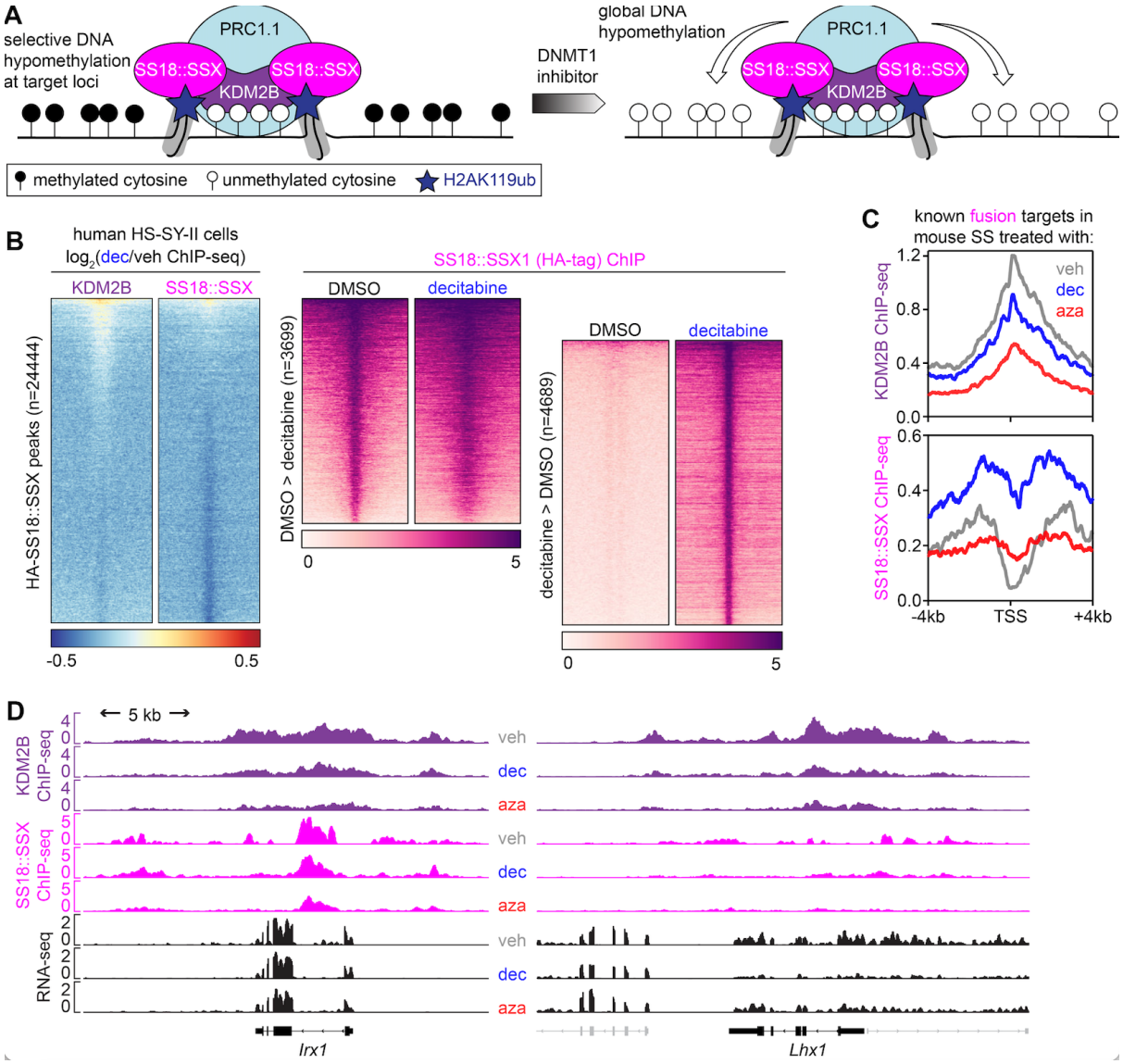

Figure 7. KDM2B redistributes upon DNMT inhibition in synovial sarcoma. (**A**) Schematic diagram illustrating the possibility of SS18::SSX redistribution with increased regions of hypomethylation following DNMT inhibitor treatment. (**B**) Left, heatmaps of the log2-transformed fold change KDM2B or SS18-SSX (endogenously HA tagged) calibrated ChIP signals in HS-SY-II cells treated with DMSO or 500nM decitabine over the total SS18-SSX peaks (DMSO and decitabine, n=24444. Rows correspond to ±10-kb regions across the midpoint of each enriched region, ranked by increasing signal. Right, heatmaps for SS18-SSX1 calibrated ChIP–seq over decreased SS18-SSX peaks (n = 3699) or gained peaks (n=4689). Rows correspond to ±10-kb regions across the midpoint of each enriched region, ranked by increasing signal. (**C**) Enrichment plots for mouse tumor ChIP-seq for KDM2B and SS18::SSX across the transcription start sites of previously confirmed target genes of the fusion following vehicle, decitabine, or azacytidine treatment (**D**) ChiP-seq track at two (rare) example target genes that showed the pattern of diminished KDM2B and fusion ChiP-seq, as well as RNA-seq.

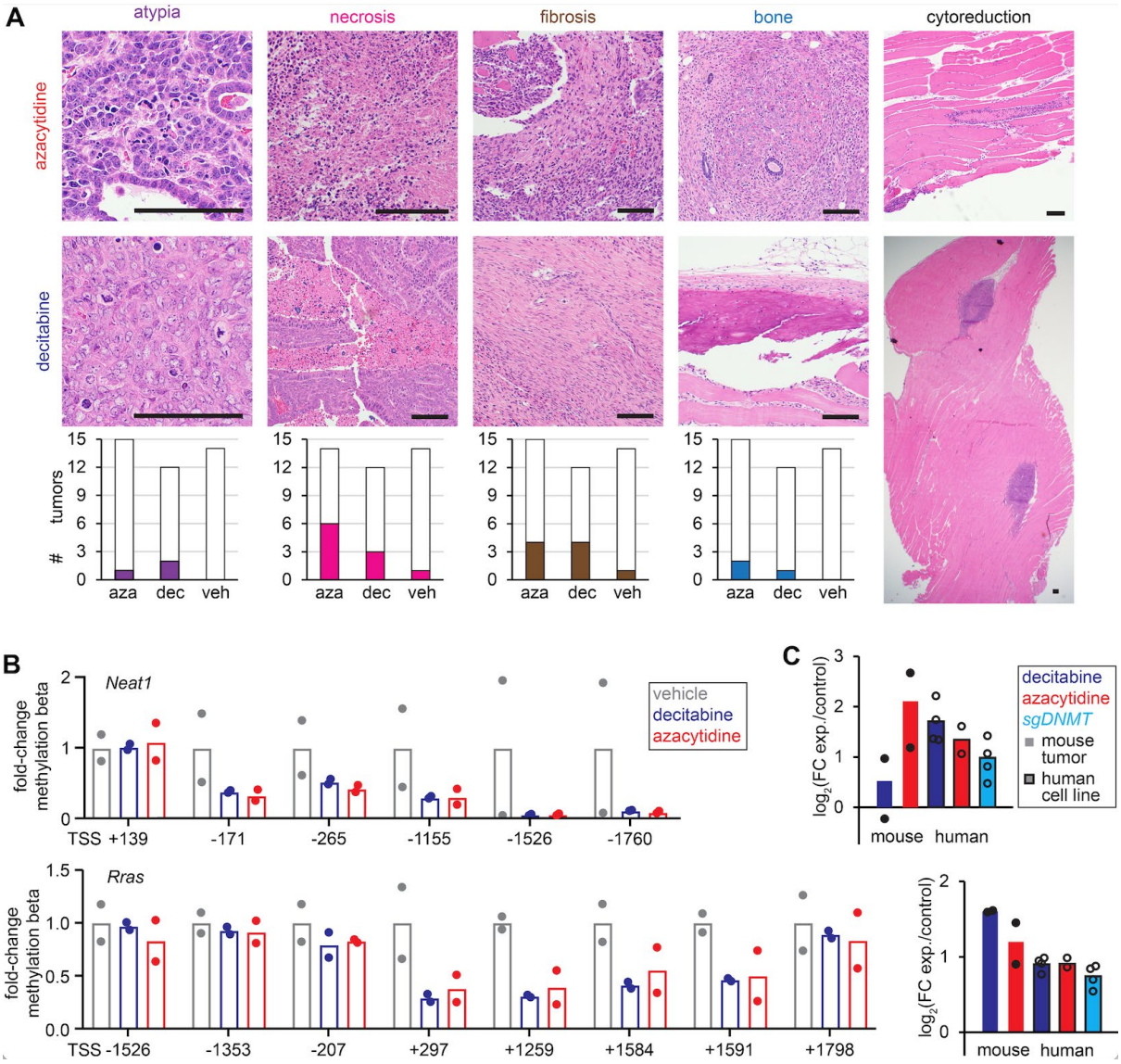

Figure 8. Changes in methylation alter mesenchymal-related and tumor-suppressor genes. (**A**) Example photomicrographs from each experimental group, as well as the prevalence of each finding across all the blindly evaluated samples from each group. Atypia, alterations in nuclear morphology and chromatin characteristics from that seen in normal cells, can be enhanced by DNA damage or cytotoxicity. Necrosis is shown by areas with abundant cells having either pyknotic (dark and small) or absent (ghost cell) nuclei with surrounding neutrophils representing an acute inflammatory response. Fibrosis is the laying down of abundant collagenous extracellular matrix between elongated spindle cells (see Supplemental Figures 3C and 6B for further visualization using Masson's trichrome). Bone formation in the form of osteoid matrix production with or without mineralization can be observed in some SSs, but was only discretely seen in azacytidine or decitabine samples in this cohort. Cytoreduction was interpreted as present when only very small areas of neoplastic cells were detectable within a background of normal host (skeletal muscle) tissue. (**B**) promoter methylation fold-changes for genes in vehicle decitabine, or azacytidine-treated tumors. (**C**) RNA-seq-determined log2-transformed fold-changes of expression.

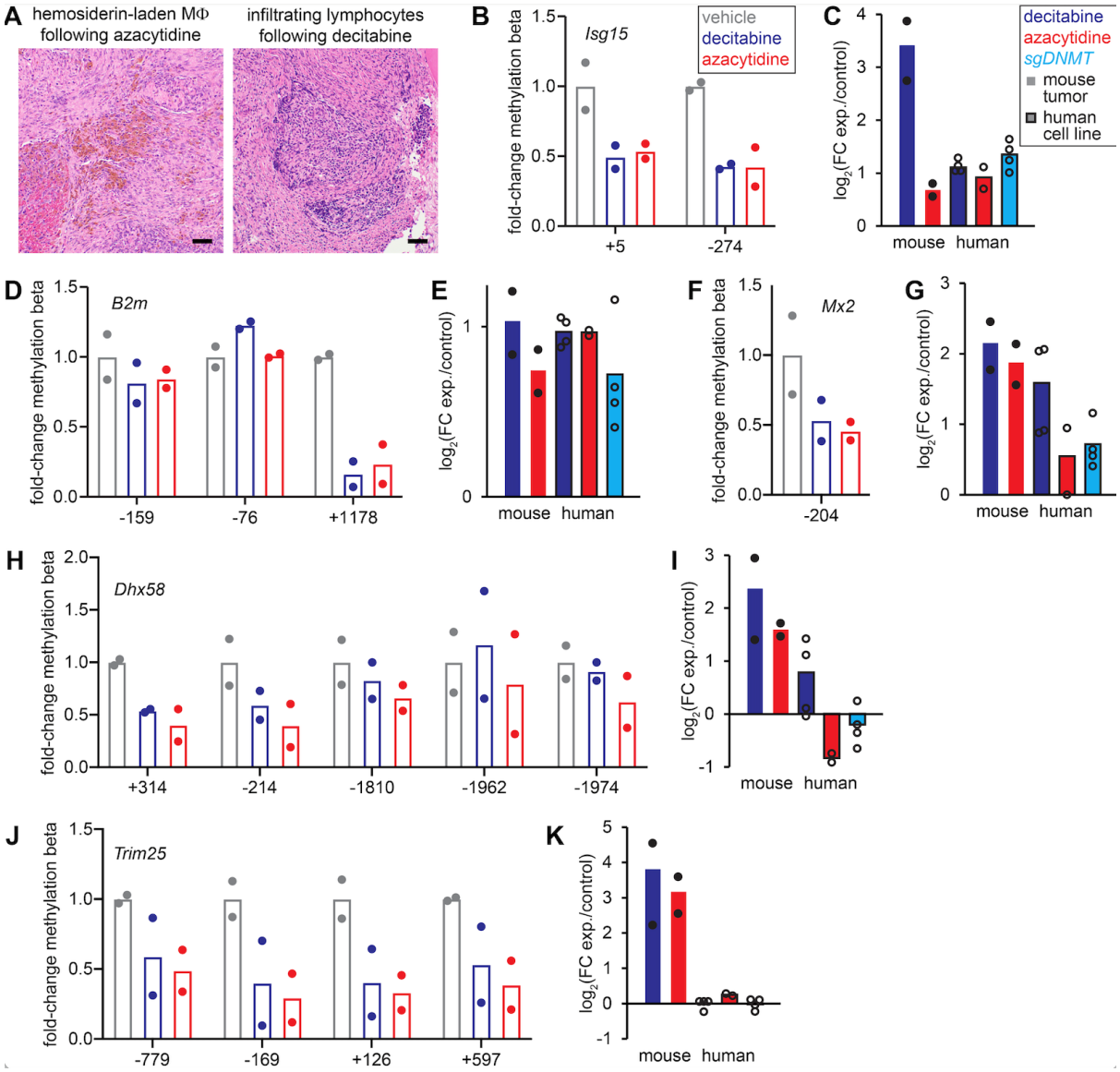

Figure 9. Changes in methylation alter immune-related genes. (**A**) Photomicrographs of H&E stained sections with abundant hemosiderin-laden macrophages (MΦ) or infiltrating lymphocytes following demethylation therapies in mouse genetically induced tumors (magnification bar is 50µm). (**B**, **D**, **F**, **H**, **I**) promoter methylation fold-changes for noted immune-related genes in vehicle decitabine, or 5-azacytidine treated tumors with matched RNA-seq-determined log2-transformed fold-changes of expression (**C**, **E**, **G**, **I**, **K**).